Cell Communication and Signaling

RESEARCH

Open Access

Acidic preconditioning induced intracellular acid adaptation to protect renal injury via dynamic phosphorylation of focal adhesion kinase-dependent activation of sodium hydrogen exchanger 1

Annan Chen[1†], Jian Zhang[1†], Zhixin Yan[1†], Yufei Lu[1], Weize Chen[1], Yingxue Sun[1], Qiuyu Gu[1], Fang Li[1], Yan Yang[1], Shanfang Qiu[2], Xueping Lin[2], Dong Zhang[2], Jie Teng[1,2], Yi Fang[1], Bo Shen[1,4*], Nana Song[1,3,4*] and Xiaoqiang Ding[1,4*]

Abstract

Background Disruptions in intracellular pH (pH_i) homeostasis, causing deviations from the physiological range, can damage renal epithelial cells. However, the existence of an adaptive mechanism to restore pH_i to normalcy remains unclear. Early research identified H^+ as a critical mediator of ischemic preconditioning (IPC), leading to the concept of acidic preconditioning (AP). This concept proposes that short-term, repetitive acidic stimulation can enhance a cell's capacity to withstand subsequent adverse stress. While AP has demonstrated protective effects in various ischemia-reperfusion (I/R) injury models, its application in kidney injury remains largely unexplored.

Methods An AP model was established in human kidney (HK2) cells by treating them with an acidic medium for 12 h, followed by a recovery period with a normal medium for 6 h. To induce hypoxia/reoxygenation (H/R) injury, HK2 cells were subjected to hypoxia for 24 h and reoxygenation for 1 h. In vivo, a mouse model of IPC was established by clamping the bilateral renal pedicles for 15 min, followed by reperfusion for 4 days. Conversely, the I/R model involved clamping the bilateral renal pedicles for 35 min and reperfusion for 24 h. Western blotting was employed to evaluate the expression levels of cleaved caspase 3, cleaved caspase 9, NHE1, KIM1, FAK, and NOX4. A pH-sensitive fluorescent probe was used to measure pH_i, while a Hemin/CNF microelectrode monitored kidney tissue pH.

†Annan Chen, Jian Zhang and Zhixin Yan contributed equally to this work.

*Correspondence:
Bo Shen
shen.bo@zs-hospital.sh.cn
Nana Song
song.nana@zs-hospital.sh.cn
Xiaoqiang Ding
ding.xiaoqiang@zs-hospital.sh.cn

Full list of author information is available at the end of the article

Immunofluorescence staining was performed to visualize the localization of NHE1, NOX4, and FAK, along with the actin cytoskeleton structure in HK2 cells. Cell adhesion and scratch assays were conducted to assess cell motility.

Results Our findings demonstrated that AP could effectively mitigate H/R injury in HK2 cells. This protective effect and the maintenance of pH_i homeostasis by AP involved the upregulation of Na^+/H^+ exchanger 1 (NHE1) expression and activity. The activity of NHE1 was regulated by dynamic changes in pH_i-dependent phosphorylation of Focal Adhesion Kinase (FAK) at Y397. This process was associated with NOX4-mediated reactive oxygen species (ROS) production. Furthermore, AP induced the co-localization of FAK, NOX4, and NHE1 in focal adhesions, promoting cytoskeletal remodeling and enhancing cell adhesion and migration capabilities.

Conclusions This study provides compelling evidence that AP maintains pH_i homeostasis and promotes cytoskeletal remodeling through FAK/NOX4/NHE1 signaling. This signaling pathway ultimately contributes to alleviated H/R injury in HK2 cells.

Keywords Acidic preconditioning, pH_i adaptation, Focal adhesion kinase, Na^+/H^+ transporter 1, NOX4, Renal epithelia cells, Cytoskeletal remodeling

Background

Intracellular pH (pH_i) is a critical determinant of the internal cellular environment. It plays a vital role in numerous physiological processes, including cell division and proliferation, enzyme activity, biomolecule expression and secretion, membrane ion transport, and endocytosis [1]. Intracellular acidosis can induce apoptosis, senescence, and ultimately cell death [2]. Extracellular acidic environments can reduce the pH_i of normal cells to suboptimal levels, hindering their function. However, cells can adapt to extracellular acidosis, overcoming this challenge [3]. Extensive research has demonstrated that repetitive, short-term acidic perfusion preconditioning is an effective strategy to induce this adaptation, a phenomenon known as acidic preconditioning (AP) [4, 5]. While some investigations suggest that H^+ may mediate ischemic preconditioning (IPC), the transport mechanisms underlying this adaptation remain poorly understood.

Cells utilize H^+-equivalent transporters to maintain a stable pH_i. These transporters include sodium/hydrogen exchangers (NHE1-9), the electrogenic Na^+-HCO_3- cotransporter (SLC4A4), the electroneutral Na^+-HCO_3- cotransporter (NBCn1), and Cl^-/HCO_3^- exchangers (CBEs; SLC4A1-3 and SLC26A6) [6]. In the renal proximal tubule, NHE1 plays a critical role as a survival factor and becomes inactivated during apoptosis [7]. NHE1 is the first cloned and most widely distributed subtype within the mammalian solute carrier family 9 A (SLC9A). Activation of NHE1 promotes the exchange of Na^+ ions into the cell and H^+ ions out of the cell across the plasma membrane. This process helps maintain homeostasis of pH_i and cellular volume, particularly under acidic intracellular conditions [8]. Interestingly, NHE1 can bind to various regulatory kinases and anchor the cell cytoskeleton. This allows NHE1 to serve as a "scaffold" for numerous signal transduction pathways influencing cellular functions like survival, migration, proliferation, and differentiation, independent of its role in ion transport. The role of NHE1 in renal diseases is complex. On the one hand, NHE1 functions as a survival factor for renal tubular epithelial cells by maintaining Akt pathway activation [9]. Conversely, adverse stimulations of NHE1 can contribute to the progression of hypertension and diabetic nephropathy [10–12]. While studies have shown a slight increase in NHE1 expression during renal ischemia-reperfusion injury (IRI), the exact role of NHE1 in this context remains unclear [13, 14]. Given NHE1's ability to sense and regulate pH_i, as well as its participation in multiple signaling pathways, it is reasonable to hypothesize that NHE1 may be involved in the acidic preconditioning of renal cells.

Focal Adhesion Kinase (FAK) is a non-motor protein associated with the cell cytoskeleton that can bind to NHE1. During integrin-mediated cell adhesion, FAK is recruited along with the actin cytoskeleton and phosphorylated proteins to form Focal Adhesions (FAs). Consequently, FAK is crucial in regulating cell adhesion, migration, proliferation, and survival [15]. FAK undergoes autophosphorylation at tyrosine residue 397 during FA formation. This creates binding sites for adaptor proteins like c-Src, p130Cas, and phosphoinositide-3 kinase, leading to further phosphorylation at sites like Y576/577 and Y925, ultimately resulting in full FAK activation. Disruption of the actin cytoskeleton and cell-extracellular matrix adhesion during acute kidney injury (AKI) leads to loss of epithelial cell polarity and detachment [16]. Studies have shown a rapid decrease in FAK phosphorylation during renal ischemia, with a gradual recovery upon reperfusion [17]. Conditional knockout of FAK in renal tubular epithelial cells during AKI has been shown to mitigate kidney damage by enhancing FA stability [18]. Additionally, inhibitors of FAK phosphorylation have the potential to alleviate the progression of AKI towards chronic outcomes [19]. Evidence suggests that pH can directly regulate the phosphorylation levels of critical FAK sites, thereby influencing cell motility [20].

For example, cardiomyocytes treated with acidic culture media exhibit increased NHE1 expression alongside a rapid decrease in FAK phosphorylation levels [5]. Furthermore, inhibiting FAK phosphorylation prevents the upregulation of NHE1 following acid stimulation. The above studies overlap in their assertion that FAK could act as a potential pH sensor, influencing NHE1 activation in the context of AP.

This study initially established an AP model that effectively mitigates H/R injuries in various renal cell lines. Subsequently, it investigates the role of the FAK/NHE1 pathway in regulating AP in vitro and IPC in vivo.

Method

Reagents and solutions

Cariporide (Cari, NHE1 inhibitor), Defactinib (Defa, FAK inhibitor), Pyrintegrin (Pyri, FAK activator), and Nigericin were purchased from Med Chem Express; Mitoquinone (MitoQ, mitochondria-targeted antioxidant), GLX351322 (NOX4 inhibitor), and Nocodazole (Noco, microtubule dynamics inhibitor) were obtained from Selleck; and N-Acetylcysteine (NAC, ROS inhibitor) was acquired from Beyotime. NAC solution was titrated with NaOH to a pH of 7.4 before use due to its intrinsic acidic pH. The components of solutions employed in this study are outlined in Table S1.

Animals experiment

The wild-type C57BL/6 mice (male, 6–8 weeks old, 20–25 g) were used in this study. Mice were housed in an acclimatized room and allowed free access to food and water. All experimental procedures were approved by the Institutional Animal Care and Use Committee of Fudan University.

The renal ischemic preconditioning (IPC) and bilateral renal ischemia-reperfusion (I/R) models in mice were based on established methods from previous research [21]. The mice were divided into four groups: sham surgery group (n=6), IPC group (n=6), bilateral ischemia-reperfusion group (n=6) and IPC+IR group (n=6). Throughout the surgery, mice were placed on a heating pad to maintain their core temperature between 36.5 °C and 37.5℃. For IPC model, mice anesthetized with 1% pentobarbital underwent abdominal incision and the bilateral renal pedicles were clamped for 15 min. The I/R procedure was conducted four days after the IPC or Sham, renal pedicles were clamped bilaterally for 35 min followed by reperfusion for a series of time points. After removal of the clamps, reperfusion was visually assessed, followed by abdominal closure. Sham-operated mice received same surgical procedures except for clamping the renal pedicles. To obtain intra-kidney pH value, the freshly collected tissue was minced with a scalpel and ground gently until it reaches a pulpy consistency. The pH meter probe was then fully immersed in the tissue to measure the pH. The kidneys were harvested 24 h after I/R for pathological and molecular biology testing.

Culture and maintenance of cells

The human proximal tubule epithelial cell line HK2 was cultured in DMEM/F12 containing 10% fetal bovine serum (FBS) and 1% penicillin/streptomycin in a humidified atmosphere of 37 °C in a 5% CO_2. The medium was changed every 2 days, and cells were passaged when confluence reached 80–90%. The medium was replaced with a serum-free culture medium for 12 h before treatment. Except for passaging, 20mM HEPES was added to the culture medium to minimize pH fluctuations during the culturing process.

The methodology for extracting primary cells was adapted from a previous study [22]. Animals were euthanized by cervical dislocation, and the bilateral kidneys were surgically removed on a sterile bench and washed three times with sterile, pre-cooled Hank's Balanced Salt Solution (HBSS) at 4 °C. The kidneys were cut into approximately 1mm^2 fragments and digested with a tissue digestion solution (collagenase and hyaluronidase in HBSS) at 37 °C for 30 min on a shaker. After filtration through a 40 μm mesh, the mixture was centrifuged at 100 g for 3 min and the pellet was further washed with HBSS. Finally, the cell pellet was resuspended in an appropriate volume of DMEM/F12 culture medium. A 50% (v/v) Percoll separation solution was carefully layered above the cell suspension to establish a distinct interface. The mixture was then centrifuged at 14,000 rpm for 1 h at 4 °C. The supernatant containing enriched PTECs was carefully aspirated, centrifuged again, and resuspended in a complete culture medium (DMEM/F12 supplemented with insulin, transferrin, vitamin C, and dexamethasone) containing 10% FBS. The isolated PTECs were seeded onto appropriate culture dishes or plates and incubated at 37 °C with 5% CO_2 for 24 h. After 24 h, the culture medium was replaced with a fresh complete medium. The cells were typically confluent (70–80% confluence) within 4–5 days of culture.

For H/R studies, the media was replaced with serum-free appropriate culture medium, and hypoxia was achieved by using an Anaeropack and sealed containers (Mitsubishi, Japan) at 37 °C, 5% CO_2, and ≤0.1% O2 for 24 h followed by 1 h of reoxygenation. To inhibit NHE1 activity during the H/R, 0.5 μm Cariporide was added 30 min prior to hypoxia. In certain experiments, 0.5 μm Cariporide was also added during the reoxygenation process.

HK2 human renal proximal tubule epithelial cells were transiently transfected with either NHE1-specific siRNA or FAK-specific siRNA to achieve knockdown of these target proteins. Lipofectamine 3000 (Invitrogen, USA)

was used for transfection, following the manufacturer's instructions. Briefly, HK2 cells were seeded in 12-well plates and cultured until they reached 80% confluence. A final concentration of 50 nM siRNA was used along with 1 μg of Lipofectamine 3000 dissolved in 500 μL Opti-MEM. Transfection efficiency was assessed 24 h post-transfection using both quantitative real-time PCR (RT-qPCR) and Western blot analysis. Subsequent treatments and experiments were then carried out 48 h after transfection.

Acidic preconditioning

To determine the optimal pH for AP in cell experiments, this study investigated the pH of kidney tissue in both I/R and IPC models. In conjunction with the findings from previous studies [4, 23, 24] and the experimental data on kidney tissue pH, a treatment pH of 6.6 was chosen for the AP cell experiments. Hydrochloric acid (HCl) and sodium hydroxide (NaOH) were used to adjust the culture medium's pH to the desired value. Additionally, 20 mM HEPES buffer was supplemented to maintain a stable pH throughout the experiment. Notably, the medium pH remained relatively constant within 24 h, with a noticeable decrease observed only after 36 h. Following the acidic medium treatment, the culture medium was replaced with a serum-free medium (pH 7.4). Subsequent experiments were then conducted after a specified recovery period. Defa, Pyri, NAC, MitoQ, and GLX351322 were added 6 h before the acidic treatment. Defa and Pyri were removed after the initiation of acidic medium treatment, while NAC, MitoQ, and GLX351322 were removed at the beginning of the acid withdrawal.

Western blotting (WB) and immunoprecipitation (IP)

For WB analysis, RIPA lysis buffer containing protease inhibitors (Merck Millipore, USA) was used to extract total proteins from HK2 cells and primary mouse proximal tubule cells. The extracted proteins were separated by 8% or 12.5% sodium dodecyl sulfate-polyacrylamide gel electrophoresis (SDS-PAGE) at 300 mA for 90 min and transferred onto polyvinylidene difluoride (PVDF, Immobilon-P; Millipore, USA) membranes under ice-cold conditions. After blocking with 5% non-fat milk at room temperature for 1 h, the membranes were incubated overnight at 4 °C with the following primary antibodies: β-actin (1:1000, Santa Cruz), NHE1 (1:500, Santa Cruz), pFAK (1:1000, CST), FAK (1:1000, CST), cleaved caspase3 (1:1000, CST), caspase3 (1:2000, Abmart), cleaved caspase9 (1:1000, CST), NOX4 (1:500, Santa Cruz), Vinculin (1:1000, Abcam), paxillin (1:1000, Invitrogen). After washing three times with TBST, the membranes were incubated in a blocking solution with the appropriate HRP-conjugated secondary antibody for 1 h at room temperature. Blots were visualized using an enhanced chemiluminescence (ECL) kit.

For IP experiments, protein samples were obtained using WB and IP lysis buffer (Beyotime, China). Protein-G magnetic beads (Thermo Fisher, USA) were incubated overnight at 4 °C with the corresponding antibody (2 μg antibody per 500 μg protein sample). After washing the beads, the proteins were eluted by incubating in 5× loading buffer at 100 °C for 10 min and subsequently analyzed by Western blot.

Immunofluorescence

The cells were seeded at a density of 1×10^5 cells per well in a 24-well cell culture plate. After fixation, permeabilization, and blocking, the cells were incubated overnight at 4℃ with primary antibodies. Following three washes, secondary antibodies were incubated at room temperature for 1 h. ActinTrackor (Beyotime, China), Alexa Fluor™ 594 DNase I (Thermo Fisher, USA) and MitoTracker™ Red CMXRos (Thermo Fisher, USA) were used for staining the F-actin, G-actin and mitochondria, respectively. DAPI was employed for nuclear staining, and mounting was done using a fluorescence quenching mounting medium. For immunofluorescence staining of kidney paraffin sections, sections underwent dewaxing, hydration and antigen retrieval. The sections were blocked and incubated with the indicated primary antibodys. The primary antibodies employed in immunofluorescence staining includes: NHE1 (1:50, Santa Cruz), pFAK (1:100, CST), NOX4 (1:500, Santa Cruz), Paxillin (1:1000, Invitrogen), COX IV (1:200, Abcam), GM130 (1:50), Calnexin (1:50), β-tubulin (1:200, ZENBIOSCIENCE), β-actin (1:500, Santa Cruz) and Lotus Tetragonolobus Lectin (LTL), Biotinylated (1:500, Vector Laboratories). Fluorescent images were captured using the FV3000 confocal microscope (Olympus, Japan), and ImageJ was used for fluorescence image processing. The Fibril Tool plugin in ImageJ was utilized to measure the anisotropy ($0< A<1$) of the actin cytoskeleton. A value of 0 indicates a completely disordered arrangement, whereas an A value of 1 reflects a perfectly aligned cytoskeletal arrangement [25].

Measurement of intracellular pH

All pH_i measurements were performed under constant conditions at 37 °C. Two fluorescent probes were employed for pH_i measurement depending on the duration of the experiment. BCECF-AM (Beyotime, China) was used for experiments requiring pH_i measurement within a 2-hour timeframe. For long-term cellular retention and assessment of pH_i changes in the same cell population pre- and post-hypoxia/reoxygenation (H/R) injury, the SNARF™-1 Carboxylic Acid, Acetate, Succinimidyl Ester probe (Thermo Fisher, USA) was utilized.

Cells were seeded in black, clear-bottomed 96-well plates and incubated with either 10 μM BCECF-AM or 10 μM SNARF-1 in HBSS for 1 h at 37 °C. Subsequently, the cells were washed three times with HBSS, and their fluorescence intensity was measured using a Varioskan™ LUX multifunction microplate reader. For BCECF-AM, the emission wavelength was set at 530 nm, and BCECF ratios were calculated as the fluorescence intensity at 490 nm excitation divided by the fluorescence intensity at 430 nm excitation. For SNARF-1, a fixed excitation wavelength of 514 nm was used, and SNARF-1 ratios were calculated as the fluorescence intensity at 580 nm emission divided by the fluorescence intensity at 630 nm emission. A standard curve generated using a calibration buffer (pH 6.9–7.6) containing 2 μM nigericin was employed to convert the fluorescence ratio to pH_i. The cellular response to extracellular acid load was evaluated using a pHe-pHi curve. Cells were cultured in sample buffers with varying pH levels (6.0, 6.2, 6.4, 6.6, 6.8, 7.0, 7.2, and 7.4) for 15 min each, followed by measurement of the corresponding pH_i.

To assess the activity of the Na^+/H^+ exchanger NHE1, an NH_4Cl prepulse technique was employed. Briefly, HK2 cells loaded with the pH-sensitive fluorescent indicator BCECF were incubated in a sample buffer for 10 min. During this incubation period, a stable baseline pH_i was measured. Subsequently, the cells were perfused with an NH4Cl buffer for 5 min. This rapid influx of ammonium chloride induced an intracellular acid load, which triggered NHE1 activity to restore pH_i homeostasis. Following the NH_4Cl exposure, the cells were returned to the original sample buffer. pH_i recovery was then monitored by measuring fluorescence every 30 s for 10 min. The initial rate of pH_i recovery ($\Delta pH_i/\Delta t$) serves as a quantitative measure of NHE1 activity.

Measurement of kidney tissue pH

The Hemin/CNF microelectrode and electrochemical analysis instruments for pH detection in kidney tissues were kindly provided by Professor Liming Zhang from the Department of Chemistry at East China Normal University, Shanghai, China. We employed differential pulse voltammetry (DPV) for electrochemical analysis using an Ag/AgCl reference electrode. DPVs were scanned from 0.0 V to −0.8 V with a step potential of 8 mV, an interval of 0.5 s, and a modulation amplitude of 50 mV. Our results demonstrated a well-defined redox peak for the Hemin/CNF microelectrode, exhibiting a linear relationship between the half-wave potential ($E_1/_2$) of Fe^{2+}/Fe^{3+} in hemin and the environmental pH (ranging from 5.36 to 8.50) (Figure S1). Following adequate anesthesia of the mice, the kidneys were surgically exposed, and the renal capsule was carefully removed. Using a stereotactic apparatus and under microscopic visualization, the microelectrode was implanted approximately 1 mm deep into the kidney tissue. DPVs were recorded at baseline (0 min) before clamping the renal pedicle and again at 15 and 35 min post-clamping. Throughout the experiment, the mice were maintained on a heating pad to ensure a body temperature of approximately 37 °C. Peak fitting and $E_1/_2$ determination were performed using OriginPro 9.0 software (OriginLab Corp., Northampton, MA, USA).

Cell viability, AnnexinV/PI staining, and Tunel staining

Cellular viability was assessed using the CellTiter-Lumi™ II luminescence-based cell viability assay kit (Beyotime, China). HK2 cells were seeded at a density of 5,000 cells per well in black 96-well plates. The cells were subjected to various pre-treatments, including acidic preconditioning, drug interventions, and hypoxia/reoxygenation (H/R) injury. Subsequently, 100 μL of CellTiter-Lumi™ II reagent was added to each well, followed by a 2-minute shaking incubation at room temperature. The luminescence intensity (Lumi) was then obtained using a multifunctional microplate reader. Cell viability was calculated as (Lumi[treatment group] / Lumi[control group]) × 100%.

To evaluate cell apoptosis, two commercially available kits were employed: the Annexin V-FITC/PI Apoptosis Assay Kit (Keygene Biotech, China) and the TUNEL Apoptosis Assay Kit (Yeason, China). For the Annexin V-FITC/PI staining protocol, cells were harvested and resuspended in a Binding Buffer at a density of 1×10^6 cells/mL. Following the manufacturer's instructions, Annexin V-FITC and PI (diluted 1:100) were added and incubated for 15 min at room temperature. Stained cells were then analyzed using an Attune™ NxT flow cytometer (Thermo Fisher, USA) and categorized as live (PI negative, Annexin V negative), early apoptotic (PI negative, Annexin V positive), late apoptotic (PI positive, Annexin V positive), and dead cells (PI positive, Annexin V negative). Data processing was performed using FlowJo software. For the TUNEL staining protocol, cells seeded in 24-well plates were fixed, permeabilized, and washed according to the manufacturer's guidelines. TUNEL staining was then performed. Images were captured using an FV3000 confocal microscope. TUNEL-positive cells were identified as those exhibiting positive staining for both TUNEL and DAPI. For the positive control group, cells were treated with DNase I for 10 min prior to TUNEL staining to induce DNA fragmentation.

Wound healing assay and adhesion assay

A wound-healing assay was employed to assess the average rate of HK2 cell migration. HK2 cells were seeded in six-well plates and allowed to reach approximately 90% confluence. To create a standardized wound, the cell monolayer was manually scratched using a 200 μL pipette

tip. The culture medium was then replaced with a serum-free medium to minimize the influence of cell proliferation on wound closure. Images of the scratches were captured at 0 and 24 h post-wounding using an inverted microscope. ImageJ software was then utilized to quantify the corresponding wound areas (S). The cell migration rate was calculated using the following formula: Cell Migration Rate %= (S[0 h] - S[24 h] / S[0 h]) × 100%.

For the cell adhesion assay, HK2 cells were seeded at a density of 5×10^4 cells per well in a 96-well plate pre-coated with fibronectin at a concentration of 10 μg/cm². The cells were allowed to adhere for 1 h in a humidified incubator at 37 °C and 5% CO_2. Following incubation, the wells were gently washed three times with PBS to remove non-adherent cells. A luminescence-based cell viability assay kit, CellTiter-Lumi™ II (manufacturer information, city, state), was used to quantify cell adhesion. Luminescence intensity was measured and directly correlates with the number of adhered cells. Wells without the washing step served as a control for the total cell number. The cell adhesion rate was calculated using the following formula: Cell Adhesion Rate %= Lumi[adhesion] / Lumi[control] × 100%.

Detection of reactive oxygen species (ROS), Superoxide Anion ($OO_2^{\bullet-}$), mitochondrial oxidative stress, and H_2O_2

DCFH-DA (2,7-Dichlorofluorescin diacetate, Beyotime, China) was used to intracellular total ROS and Mitosox Red probe (Invitrogen, USA) is defined as indicator of mitochondrial oxidative stress. $O_2^{\bullet-}$ and H_2O_2 levels was measured by DHE (Dihydroethidium, Beyotime, China) and Hydrogen Peroxide Assay Kit (Beyotime, China).

Cells were seeded onto a black, bottom clear 96 well plate. 10 μM DCFH-DA, 5 μM DHE, or 500 nM Mitosox Red in HBSS was added. The plate was incubated at 37 °C in a 5% CO2 incubator for 20 min and washed three washes with HBSS. A multifunctional microplate reader was used to measure the corresponding fluorescence intensity (Flou). Excitation and emission wavelengths for DCFH-DA, DHE, and Mitosox Red were 490/520, 300/610, and 396/610, respectively. Subsequently, images were captured using an inverted fluorescent microscope. Finally, protein concentration per well (μg) was determined by BCA assay, allowing for the correction of fluorescence intensity (Flou/μg).

For H_2O_2 detection, cells were lysed, and the supernatant was collected after centrifugation. H_2O_2 Detection Reagents was added to the samples and allowed to react at room temperature for 30 min. The absorbance at 560 nm was measured and H_2O_2 level in the samples was determined using a standard curve from a serial concentration of H_2O_2 ranging from 0.5 μM to 5 umol.

Statistics

The data in this study are presented as mean ± standard deviation. GraphPad Prism (GraphPad Prism 9.3.0 for MacOS; GraphPad, Bethesda, MD) was employed for data analysis and visualization. Unpaired t-tests and one-way ANOVA tests were conducted to determine statistical significance between two and multiple groups, respectively. For multiple comparisons in the one-way ANOVA, Tukey's post-hoc test was used. Differences between groups were considered statistically significant when $P \leq 0.05$.

Results

AP treatment alleviates H/R-induced injury

While previous research has demonstrated the protective effects of AP in neurons and cardiomyocytes, its impact on renal epithelial cells remains unclear. To investigate the potential protective role of AP in this context and determine the most effective preconditioning scheme (including degree, duration, and recovery period of acidic treatment), we confirmed that intra-kidney pH decreased to a range of 6.49–6.71 following effective IPC treatment (Fig. 2D). Based on existing literature reporting AP protocols for other cell types with a pH range of 5.97-7.0, we employed an acidic culture medium at pH 6.6 to pre-treat HK-2 cells before subjecting them to H/R injury. To optimize the AP protocol, the process was divided into two stages: (1) Acidic treatment (A): exposure to acidic culture medium (pH 6.6) and (2) recovery (R): replacement with normal culture medium (pH 7.4) (Fig. 1A). Initially, HK-2 cells were treated with an acidic medium (pH 6.6) for varying durations (1 h, 6 h, 12 h, and 24 h) (A1-A24), followed by a 3-hour recovery period (R3) before H/R. Compared to the control group (normal culture medium), acidic treatment for 12 h (A12R3) significantly reduced apoptosis markers (cleaved-caspase3/9) and improved cell viability after H/R (Fig. 1B, C). To determine the optimal recovery time, we fixed the acidic treatment duration at 12 h (A12) and tested various recovery times (3 h, 6 h, and 12 h) (R3-R12) before H/R exposure. The results revealed that the A12R6 (12 h acidic treatment followed by 6 h recovery) scheme exhibited the lowest level of apoptosis markers and the highest cell viability following H/R (Fig. 1D, E). Further analysis with TUNEL staining and flow cytometry confirmed that A12R6 significantly reduced apoptosis in HK-2 cells after H/R (Fig. 1F, G). Similar results were observed in murine PTECs (Figure S1). In conclusion, our findings demonstrate that the A12R6 protocol significantly attenuates H/R-induced damage in renal epithelial cells. This optimized protocol will be employed as the primary method for AP in subsequent experiments. In the following text, unless otherwise specified, AP will refer to the A12R6 protocol.

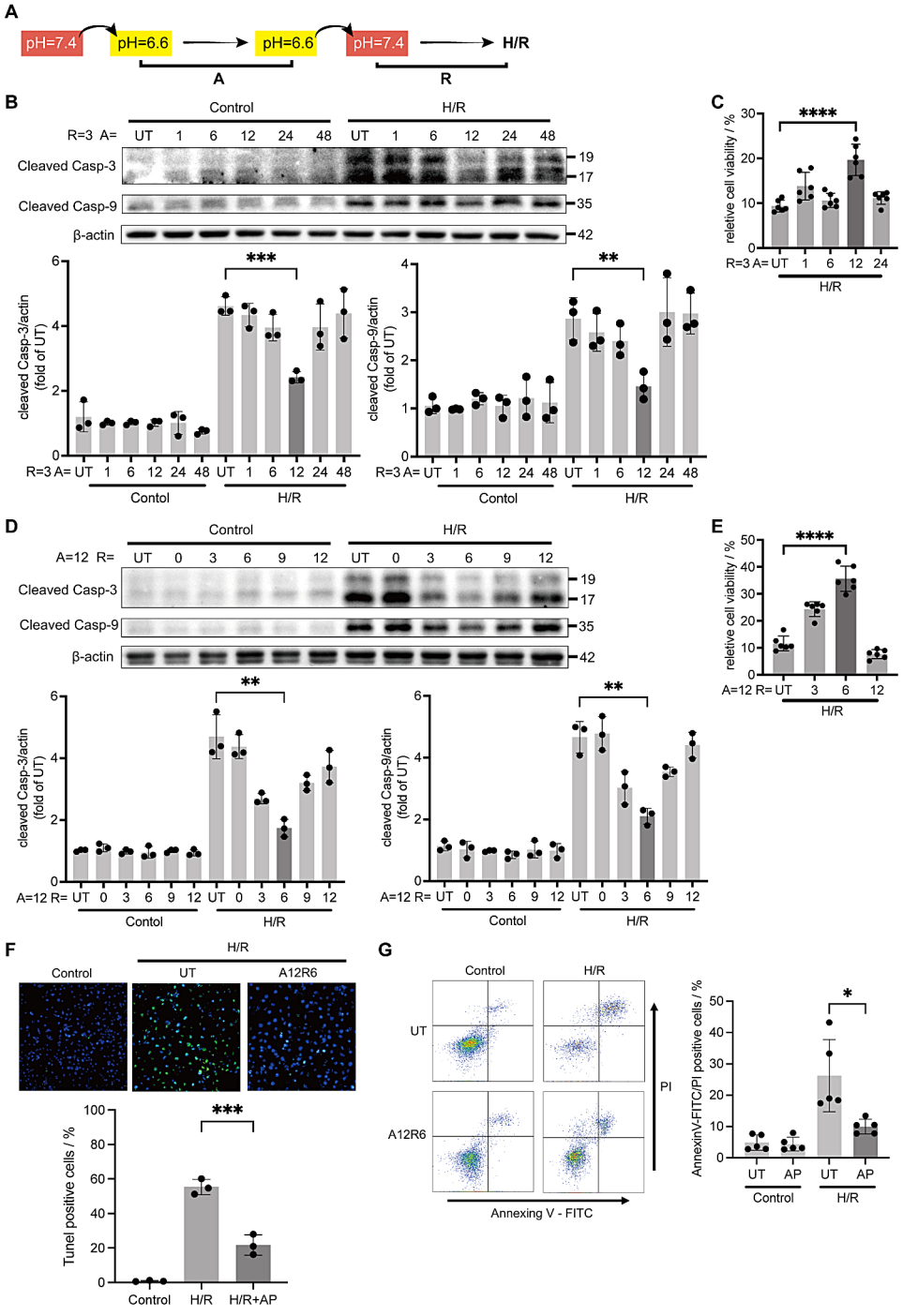

Fig. 1 Establishment of an acidic preconditioning model. (**A**) Schematic diagram of AP. HK2 cells were subjected to an acidic treatment phase (pH 6.6 culture medium) followed by a recovery phase (pH 7.4 culture medium) before H/R treatment. (**B** and **C**) Immunoblots of cleaved caspase3 (cleaved Casp-3), cleaved caspase9 (cleaved Casp-9) and β-actin (used as a loading control) expression and quantitative analysis in HK2 cells after H/R injury, with different durations of acidic medium treatment (1 h, 6 h, 12 h, and 24 h; A1-A24) and a 3-hour recovery time (R3, $n=3$). Cell viabilities at the corresponding time points were measured using CellTilter (C, $n=6$). (**D** and **E**) Immunoblots of cleaved Casp-3 and cleaved Casp-9 expression and quantitative analysis in HK2 cells at different recovery times after H/R injury, when treated with a 12-hour duration of acidic medium (A12) and different durations of recovery time (0 h, 3 h, 6 h, 9 h and 12 h; R0-R12; $n=3$). Cell viabilities at the corresponding time points were measured using CellTilter (E, $n=6$). (**F** and **G**) Tunel ($n=3$) and Annexin V-PI staining ($n=6$) were used to detect the apoptosis level of A12R6-treated HK2 cells after H/R injury. All data are expressed as mean ± SEM. $^{*}p<0.05$, $^{**}p<0.01$, $^{***}p<0.001$, $^{****}p<0.0001$. One-way ANOVA followed by Sidak's post test was used for multiple comparisons

AP alleviates H/R-induced damage via maintaining pHi Homeostasis and upregulating NHE1 expression and activity

Hypoxia exposure leads to a reduction in pH_i, while AP pretreatment mitigates this hypoxia-induced intracellular acidosis (Fig. 2A and B). Furthermore, the time course of pH_i following reoxygenation demonstrates that while pH_i in both control and AP-pretreated cells gradually returns to normal after hypoxia, AP-pretreated cells recover their baseline pH_i significantly faster (30 min vs. 90 min) (Fig. 2B). Additionally, AP treatment elevates the pH_e-pH_i curve of HK2 cells (Fig. 2C). In vivo experiments revealed that renal ischemia reduces both renal tissue pH and renal tubular pHi. However, IPC treatment blunts the ischemia-induced decrease in pH_i without affecting renal tissue pH (Figure S2 and Fig. 2D and E). Notably, IPC also significantly shifts the pH_e-pH_i curve of renal epithelial cells upwards (Fig. 2F). These data collectively suggest that AP may protect against H/R injury by maintaining pH_i homeostasis.

NHE1 is a critical mechanism for extruding H^+ ions during intracellular acidosis. To investigate its role in maintaining pH_i homeostasis after AP, we measured NHE1 expression and activation. Our findings revealed that NHE1 expression upregulated following acidic treatment, with the peak occurring at the A12R6 protocol (Fig. 3A, B). This suggests NHE1 involvement in AP-mediated pH_i elevation. Notably, IPC treatment also significantly increased NHE1 expression while decreasing the kidney injury marker KIM-1 and reducing renal cell apoptosis after I/R (Fig. 3C). Immunofluorescence staining of kidney tissue in the IPC group after I/R demonstrated a higher degree of co-localization between NHE1 and LTL (a marker of the proximal renal tubule) (Fig. 3D). Additionally, NHE1 activity significantly increased following AP. To confirm NHE1's role in pH_i tolerance and AP's protective effect, we employed

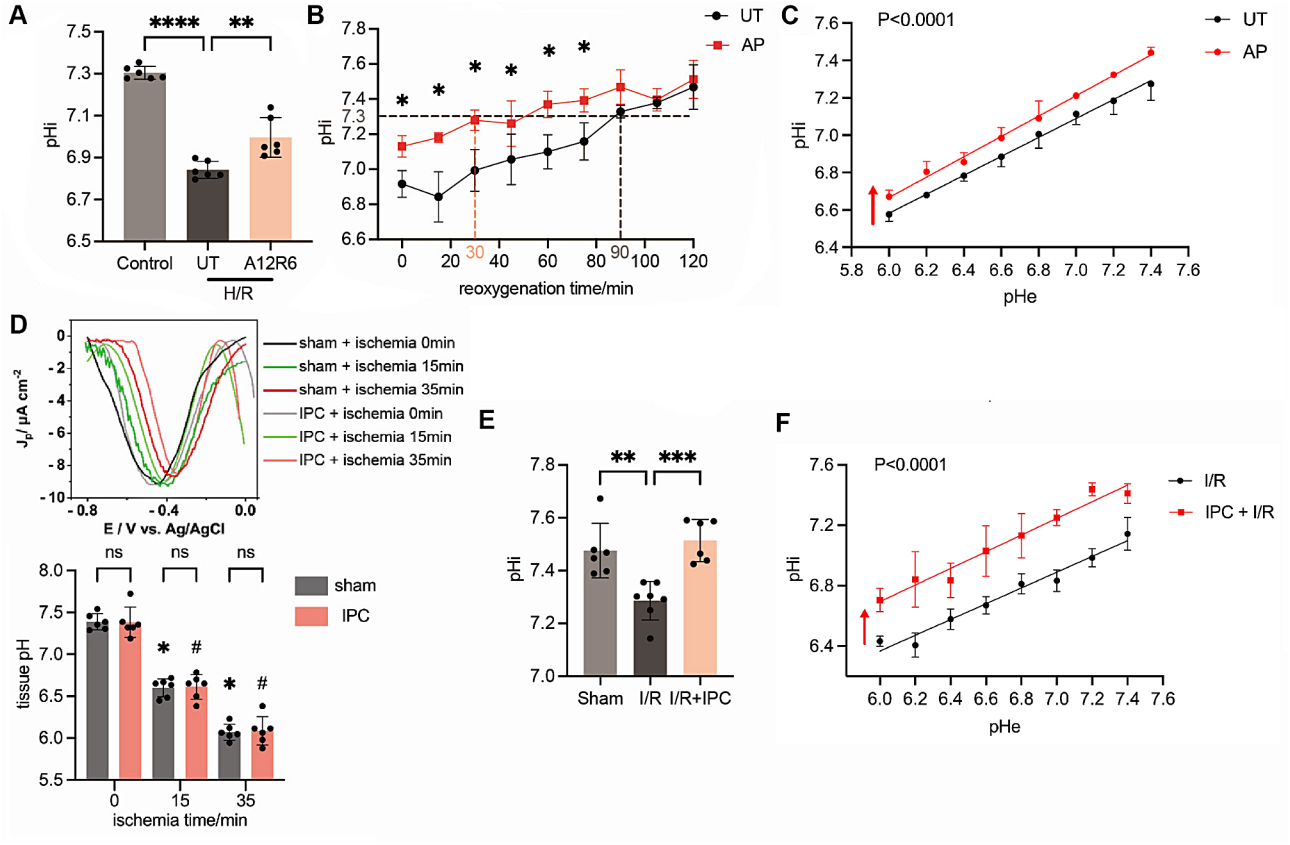

Fig. 2 The maintenance of pHi Homeostasis by AP. (**A**) HK2 cells in the control group and AP group were exposed to hypoxia for 24 h, the changes in pHi of over time were detected during the reoxygenation phase ($n=4$). pH = 7.3 was considered as the normal pHi. (**B**) The pHi of HK2 cells in the control group and AP group after H/R injury ($n=6$). (**C**) The pHe-pHi curves of HK2 cells in the control group and AP group ($n=4$). (**D**) Electrochemical analysis was used to determine kidney tissue pH of wild-type mice before clamping the renal pedicle (0 min), and 15 min and 35 min after clamping ($n=3$). (*) indicates a significant difference from the sham + 0 min group, while (#) indicates a significant difference from the IPC + 0 min group. (**E**-**F**) The pHi (E, $n=4$) and pHe-pHi curves (F, $n=4$) of isolated proximal tubular epithelial cells of control and IPC treated mice after I/R. All data are expressed as mean ± SEM. Asterisks denote statistical significance: *$p<0.05$, **$p<0.01$, ***$p<0.001$. Significance testing was performed using unpaired Student's t-test and One-way ANOVA followed by Sidak's post test

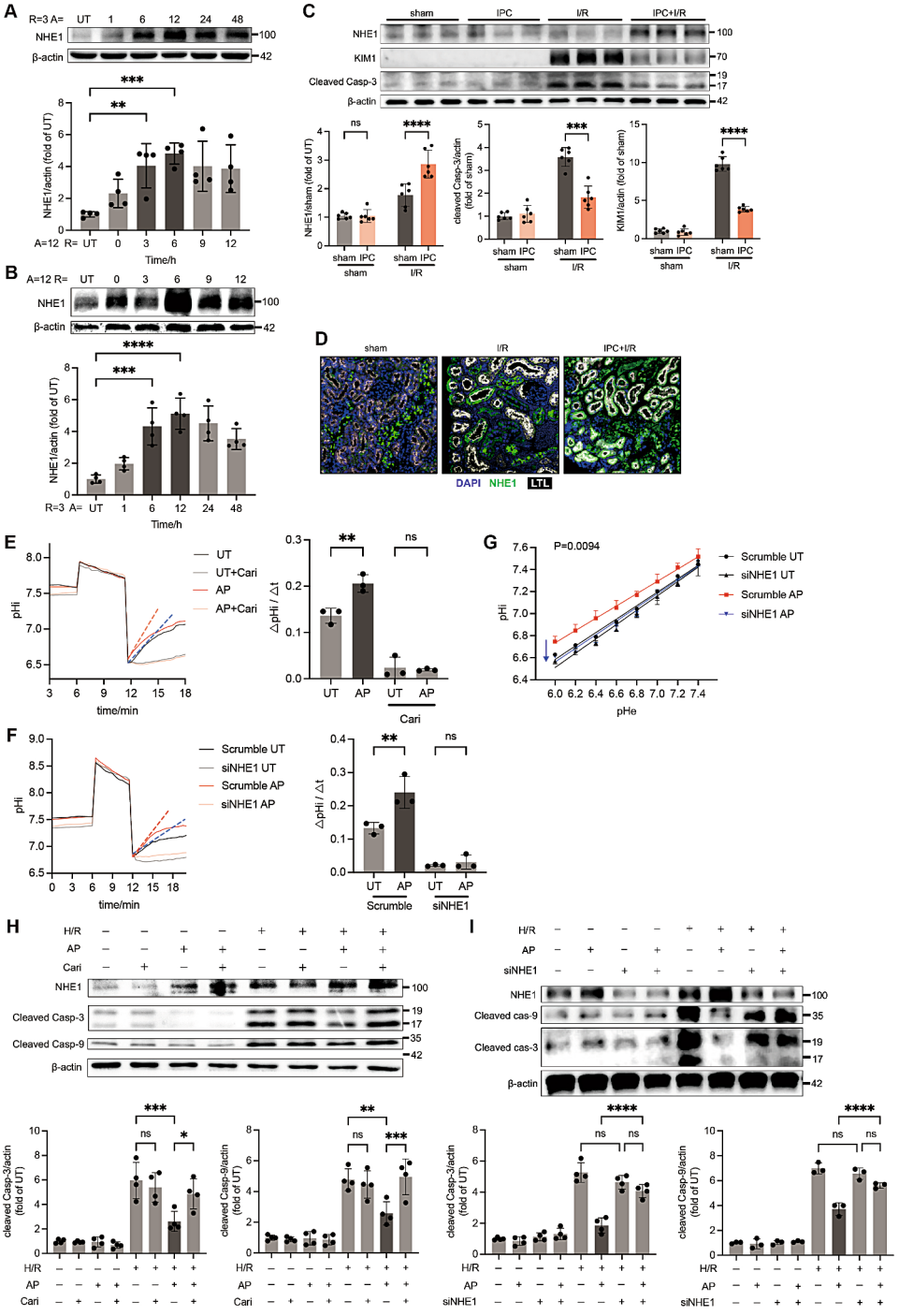

Fig. 3 AP upregulates NHE1 expression and transport activity. (**A**-**B**) Immunoblots of NHE1 expression and quantitative analysis in HK2 cells after treatment with acidic medium for different times (1 h, 6 h, 12 h, and 24 h; A1-A24), with a 3-hour recovery time(A, $n=6$). NHE1 Immunoblots of NHE1 expression in HK2 cells at different recovery times (0 h, 3 h, 6 h, 9 h and 12 h; R0-R12) were also measured after a 12-hour acidic medium treatment time (B, $n=6$). (**C**) Immunoblots of NHE1, Kim1, and cleaved Casp-3 expression and quantitative analysis in control and IPC treated mice after I/R ($n=6$). (**D**) Immunofluorescence staining revealed increased expression of NHE1 (green, anti-NHE1) in the proximal tubule (white, LTL) in kidney tissue after I/R in IPC treated mice. (**E**-**F**) The NHE1 activity of HK2 cells in the control group and AP group was measured by NH4Cl prepulse method after treatment with 0.5μM Cariporide (E, $n=3$) or after knocking down NHE1 (F, $n=3$). The dashed lines in the figure represents the pH recovery rate after intracellular acid loading, which is used to reflect NHE1 activity. (**G**) The pHe-pHi curves of HK2 cells in the control group and AP group were obtained after knocking down NHE1 ($n=4$). (**H**-**I**) Cariporide was utilized to inhibit NHE1 activity (H, $n=4$), while small interfering RNA (I, $n=4$) was employed to knock down NHE1 expression in HK2 cells in the control group and AP group, respectively, prior to H/R treatment. Western blotting was utilized to assess the expression of cleaved cas-3 and cleaved cas-9 in HK2 cells following the treatment. All data are expressed as mean ± SEM. Asterisks denote statistical significance: *$p<0.05$, **$p<0.01$, ***$p<0.001$, ****$p<0.0001$. Statistical significance was determined using one-way ANOVA followed by Sidak's post test

Cariporide and siRNA-NHE1 to inhibit or knockdown NHE1, respectively. Knockdown of NHE1 by siRNA was verified using PCR and Western blotting (Figure S3). As expected, NHE1 inhibitor Cariporide (Fig. 3E) and NHE1 knockdown with siRNA (Fig. 3F) counteracted NHE1 activation. Consequently, the shift in the pH_e-pH_i curve observed after AP treatment with NHE1 was also abolished by NHE1 knockdown (Fig. 3G). Interestingly, while neither inhibiting nor reducing NHE1 expression noticeably affected H/R damage, both actions weakened the protective effect of AP (Fig. 3H, I). These results strongly suggest that AP maintains pH_i homeostasis through NHE1 stimulation, thereby eliciting a protective effect on H/R damage.

AP upregulates NHE1 expression and activity through transient fluctuation in pHi following acid stimulation

A decrease in pH_i serves as a stimulatory feedback mechanism for NHE1. To investigate whether AP mediates NHE1 activation by reducing pH_i, we monitored the dynamic changes in pH_i within HK2 cells treated with an acidic medium (pH 6.6). Our findings revealed a rapid decrease in pH_i immediately following acidic treatment. Subsequently, pHi gradually recovered and eventually surpassed control group levels after approximately 30 min (Fig. 4A). It is established that reducing the chloride (Cl^-) concentration in the culture medium intrinsically elevates intracellular bicarbonate (HCO_3^-) concentration, thereby increasing pH_i. To confirm the role of reduced pH in NHE1 activity, a low-chloride medium was employed to neutralize the AP-induced decrease in pH_i (Fig. 4A). As expected, treatment with a low-chloride medium reversed the increase in NHE1

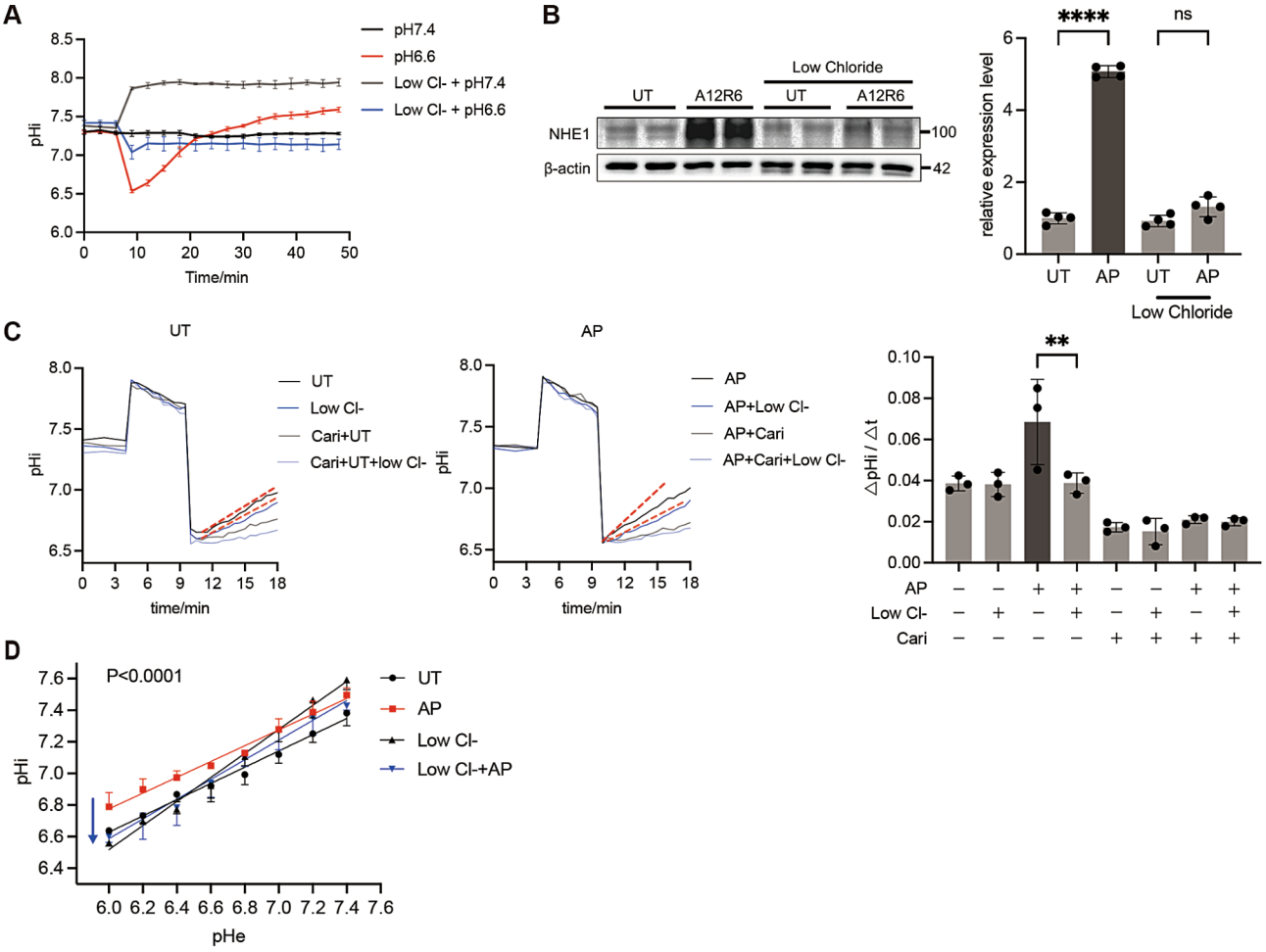

Fig. 4 Transient fluctuation in pHi following acid stimulation upregulates NHE1 expression and activity. (**A**) Changes in pHi over time in HK2 cells cultured in normal (pH = 7.4 and pH = 6.6, $n = 4$) and low chlorine media (pH = 7.4 and pH = 6.6, $n = 4$). (**B**-**D**) AP was performed in HK2 cells cultured in normal chloride ion medium and low ion medium, respectively. The NHE1 protein expression level (**B**, $n = 4$), transport activity (**C**, $n = 3$), and pHe-pHi curve (**D**, $n = 4$) of HK2 cells was obtained. All data are expressed as mean ± SEM. Asterisks denote statistical significance: $^*p < 0.05$, $^{**}p < 0.01$, $^{***}p < 0.001$. Statistical significance was determined using unpaired Student's t-test and One-way ANOVA followed by Sidak's post test

expression and activity observed after AP (Fig. 4B, C), along with the shift in the pH_e-pH_i curve (Fig. 4D). These findings collectively suggest that AP triggers a transient drop in pHi, leading to NHE1 activation. Subsequently, NHE1 extrudes H^+ ions to restore and maintain pHi homeostasis.

Activation of NHE1 is dependent on dynamic changes in FAK phosphorylation levels

FAK, a member of the non-receptor protein tyrosine kinase family, may function as a potential pH sensor. This is because its autophosphorylation sites at Y397 are known to be regulated by pH_i. To investigate the impact of an acidic culture medium on FAK Y397 phosphorylation, HK2 cells were treated with media at pH 6.6, pH 6.9, and pH 7.4 for various durations (10 min, 30 min, 1 h, and 24 h). Results showed a significant decrease in Y397 phosphorylation levels at 10 and 30 min after pH 6.6 treatment, returning to control levels after 1 h (Fig. 5A). This aligns with the observed dynamic changes in pH_i following acidic treatment. To further explore FAK's role in AP, Defactinib (a FAK Y397 phosphorylation-specific inhibitor) and Pyrintegrin (an agonist) were employed. These drugs triggered the sustained inhibition or activation of FAK Y397 phosphorylation, respectively, and mitigated the initial fluctuations in Y397 phosphorylation levels observed after acidic treatment (Fig. 5B). Interestingly, both inhibiting and stimulating FAK Y397 phosphorylation significantly attenuated the AP-mediated upregulation of NHE1 expression (Fig. 5C). Knockdown of FAK produced similar effects (Fig. 5D). Additionally, both drugs mitigated the protective effect of AP against H/R-induced damage in HK2 cells, evidenced by reduced cell viability and accelerated apoptosis (Fig. 5E-H). Taken together, these findings suggest that the dynamic changes in FAK phosphorylation, rather than simply its phosphorylation or dephosphorylation state, are crucial for the protective role of AP. As shown in Figure S4, the phosphorylation levels of FAK were altered after 6 h of exposure to Defactinib and Pyrintegrin, with the effects regressing 6 h after thorough washout. Based on this observation, a treatment scheme involving sequential application of Defactinib (6 h) and Pyrintegrin (6 h) was designed to mimic the AP-induced fluctuations in Y397 phosphorylation. As expected, this scheme significantly increased NHE1 expression levels and channel activity compared to treatments with continuous inhibition or slow recovery of FAK phosphorylation (Fig. 5I, J). Furthermore, this scheme offered protection against H/R injury similar to AP treatment (Fig. 5K). These results collectively support the hypothesis that the short-term fluctuations in FAK Tyr397 phosphorylation levels, mediated by pH_i changes after AP, act as a trigger for activating the protective effects of AP.

FAK activates NHE1 by inducing NOX4-mediated ROS production

It is widely thought that ROS may play a critical role in mediating the effects of AP. To investigate this possibility, we monitored ROS levels in HK2 cells using DCFH-DA and MitoSOX at various time points following acidic treatment. Our findings revealed a rapid and sustained increase in both total intracellular ROS and MitoSOX fluorescence intensity (Fig. 6A, B). Interestingly, Defactinib and Pyrintegrin, reagents that disrupt the short-term fluctuations in FAK Y397 phosphorylation after AP, also prevented ROS elevation (Fig. 6A, B). These results suggest that the increase in endogenous ROS might be a downstream consequence of the AP-induced fluctuations in FAK Y397 phosphorylation. Within cells, ROS primarily exist in two forms: free radicals ($O_2^{\bullet -}$) and non-radicals (H_2O_2). Notably, the data demonstrated a significant increase in ROS levels after AP, specifically with elevated H_2O_2 levels, while $O_2^{\bullet -}$ levels remained unchanged (Fig. 6C, D). The mitochondrial respiratory chain and the NOX family are the primary sources of endogenous H_2O_2. Among the NOX family members, NOX4 is the main subtype found in renal tubular epithelial cells, and it is uniquely capable of directly producing H_2O_2. To further identify the main source of H_2O_2 during AP, various ROS scavengers were employed: non-specific scavenger NAC, selective mitochondrial scavenger MitoQ, and NOX4 inhibitor GLX351322. Both NAC and GLX351322 effectively mitigated AP-induced H_2O_2 generation, while MitoQ had no effect on H_2O_2 levels (Fig. 6D). This suggests that NOX4 might be the primary source of ROS during AP. Notably, the application of NAC and GLX351322 abolished the protective effects induced by AP, while MitoQ did not (Fig. 6E-H). These findings further strengthen the connection between increased ROS levels and AP.

(**D**) H_2O levels were detected in HK2 cells after AP. During AP, a variety of compounds including 5mM Nac (non-selective ROS scavenger), 5μM mitoQ (mitochondria-targeted ROS scavenger), or 10μM GLX351322 (NOX4 specific inhibitor, $n=4$) were employed. (**E-H**) The application of 5mM Nac, 5μM mitoQ, or 10μM GLX351322 in the acidic treatment phase abolished the protective effect of AP in improving cell viability (E, $n=6$) and reducing the level of cleaved Casp-3 and cleaved Casp-9 expression (F, $n=6$), Tunel and Annexin V positive cells (G-H, $n=6$) after H/R. All data are expressed as mean±SEM. Asterisks denote statistical significance: $^*p<0.05$, $^{**}p<0.01$, $^{***}p<0.001$, $^{****}p<0.0001$. Significance testing was performed using unpaired Student's t-test and One-way ANOVA followed by Sidak's post test.

To elucidate the role of NOX4 in response to AP, we further investigated its expression and localization. We observed a significant increase in NOX4 protein

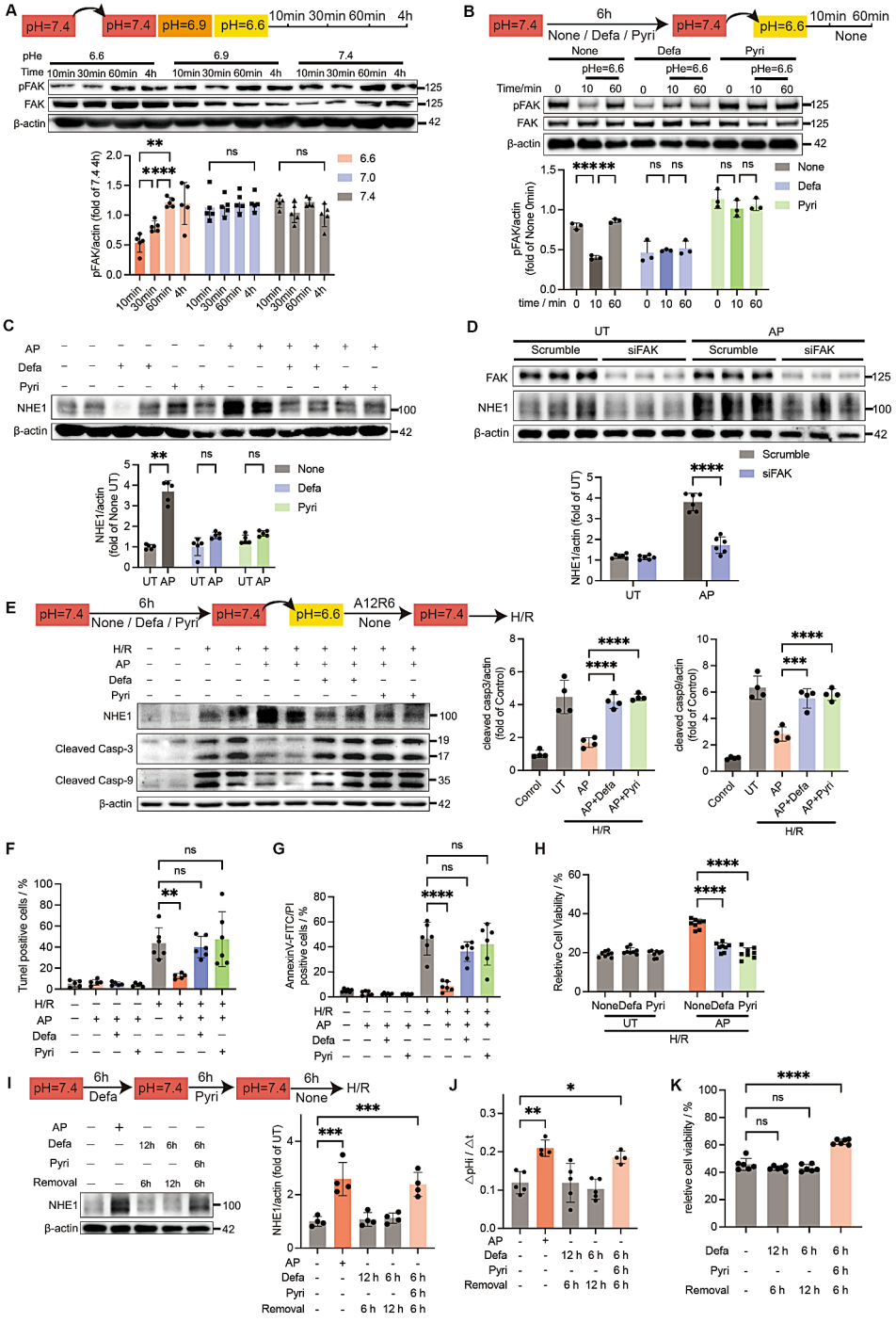

Fig. 5 Regulation of NHE1 activity by dynamic changes in FAK phosphorylation levels. (**A**) Immunoblots of FAK Y397 phosphorylation levels and quantitative analysis over time (10 min, 30 min, 60 min and 4 h) after treatment with different pH media (pH = 7.4, 6.9 and 6.6; $n = 5$). (**B**) Immunoblots were used to detect the effects of 10μM Defactinib and 0.1μM Pyrintegrin on changes in FAK phosphorylation levels and quantitative analysis after acidic medium treatment (pH = 6.6 for 10 min, 30 min, 60 min and 4 h; $n = 5$). (**C**-**D**) Immunoblots were used to detect the effect of using 10μM Defactinib and 0.1μM Pyrintegrin (C, $n = 5$) or knocking down FAK (D, $n = 6$) on NHE1 expression and quantitative analysis in HK2 cells after AP. (**E**-**H**) The application of 10μM Defactinib and 0.1μM Pyrintegrin abolished the protective effect of AP in reducing the level of cleaved Casp-3 and cleaved Casp-9 expression (E, $n = 3$), Tunel and Annexin V positive cells (F-G, $n = 3$) and improving cell viability (H, $n = 6$) after H/R injury. (**I**-**K**) 10 μM Defactinib and 0.1 μM Pyrintegrin were sequentially utilized to mimic the dynamic changes in FAK phosphorylation levels after acidic medium treatment, which upregulated NHE1 expression level (I, $n = 4$) and transport activity (J, $n = 5$), and improved the viability of HK2 cells after H/R (K, $n = 6$). All data are expressed as mean ± SEM. Asterisks denote statistical significance: *$p < 0.05$, **$p<0.01$, ***$p<0.001$, ****$p<0.0001$. Significance testing was performed using unpaired Student's t-test and One-way ANOVA followed by Sidak's post test

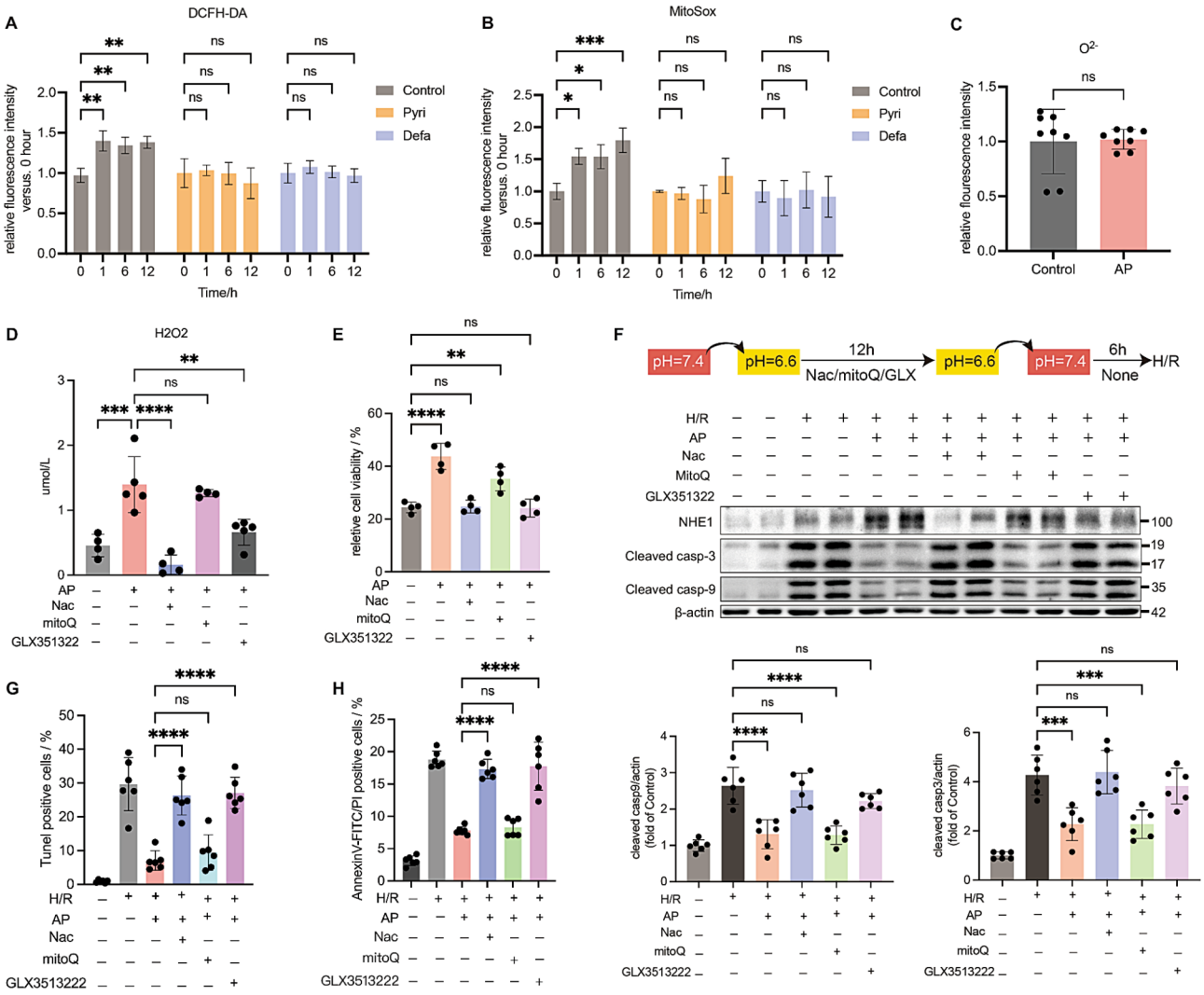

Fig. 6 NOX4 is identified as the main source of ROS during AP. (**A**-**B**) HK2 cells were treated with acidic medium with or without 10μM Defactinib and 0.1μM Pyrintegrin for different time periods (0, 1, 6, 12 h). DCFH-DA and MitoSox were used to detect total intracellular ROS (A, $n=3$) and mitochondrial oxidative stress level (B, $n=3$). (**C**) DHE was used to detect $O_2^{\bullet-}$ levels in control and AP treated HK2 cells($n=8$)

expression following AP. Interestingly, inhibiting the fluctuation of FAK Y397 phosphorylation during AP abolished the upregulation of NOX4 (Fig. 7A). Furthermore, treatment with NAC and GLX351322 during the acidic treatment phase effectively suppressed the increase in NHE1 expression and activity in HK2 cells (Fig. 7B and C). Immunofluorescence staining revealed that NOX4 predominantly localized to mitochondria in untreated HK2 cells (Figure S5). Following AP, colocalization of NOX4 with NHE1, paxillin, phosphorylated FAK (p397 FAK), and paxillin was observed (Fig. 7D). This phenomenon was also evident in PTECs (Figure S6). Co-IP experiments further confirmed interactions between NHE1 and NOX4, paxillin, p397 FAK, actin, CK18, and vimentin, but not with β-tubulin (Fig. 7E). These findings suggest that AP triggers the formation of a complex at focal adhesions composed of FAK, NOX4, and NHE1, potentially influencing cytoskeletal remodeling.

AP induces actin skeleton remodeling by FAK-NOX4-NHE1 pathway

FAK is known to bind and activate various proteins at focal adhesions, ultimately promoting cell migration, proliferation, and survival. Phalloidin staining revealed that HK2 cells exhibited a rearrangement of cortical actin after AP. Previously straight actin bundles transformed into stress fibers extending from the cytoplasm towards the plasma membrane, resulting in the formation of spike-like structures. Notably, the anisotropy of the actin cytoskeleton, a measure of its directional organization, significantly increased after AP (Fig. 8A). Actin cytoskeletal remodeling is associated with the assembly and maturation of FAs. Interestingly, our data demonstrated

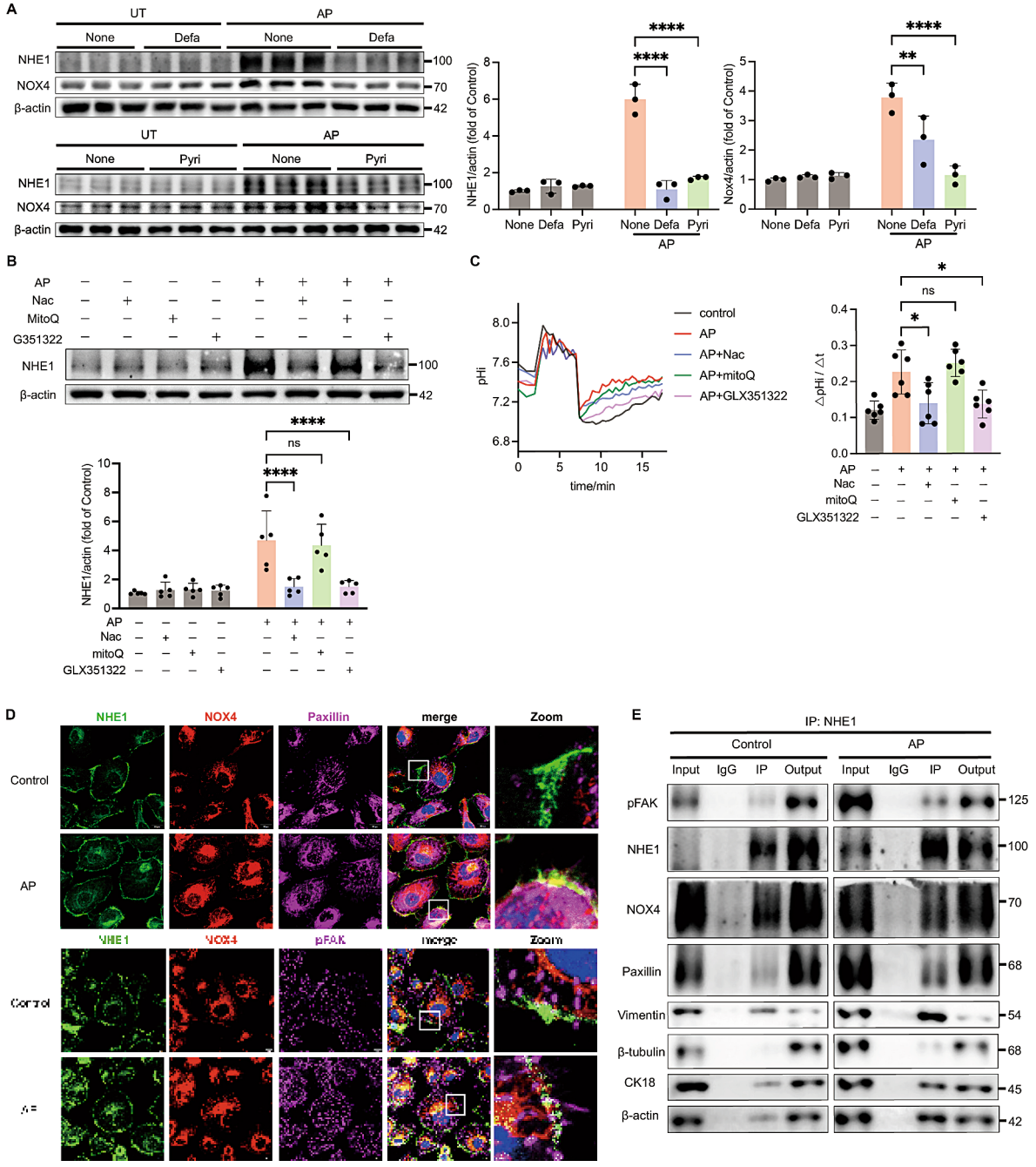

Fig. 7 AP activates NHE1 through FAK-NOX4 signaling. (**A**) Immunoblots were used to detect the effects of 10 μM Defactinib and 0.1 μM Pyrintegrin on NOX4 expression levels in HK2 cells after AP ($n=3$). (**B**-**C**) NHE1 protein expression levels (E, $n=5$) and transport activity (F, $n=6$) were measured after AP while 5mM Nac, 5μM mitoQ, or 10μM GLX351322 were used in the acidic treatment phase of AP. (**D**) Immunofluorescence staining shows the colocalization of NHE1 (green, anti-NHE1), NOX4 (red, anti-NOX4), paxillin, and pFAK (magenta, anti-paxillin and anti-pFAK) in AP treated HK2 cells. (**E**) Co-immunoprecipitation shows the interaction between NHE1 and pFAK, NOX4, paxillin, vimentin, CK18 and actin. All data are expressed as mean ± SEM. Asterisks denote statistical significance: *$p<0.05$, **$p<0.01$, ***$p<0.001$, ****$p<0.0001$. Significance testing was performed using unpaired Student's t-test and One-way ANOVA followed by Sidak's post test

that phosphorylated FAK (pFAK) Y397 levels continued to increase even after the initial dynamic changes observed within the first hour following AP (Fig. 8B). Co-staining with pFAK (Y397) and phalloidin revealed a widespread co-localization of activated FAs with stress fibers, particularly at protrusions formed by stress fibers at the plasma membrane after AP (Fig. 8C). Furthermore, immunofluorescence staining of Paxillin, a marker of mature FAs, revealed a significant increase in both the size and number of mature FAs (area ≥ 4μm^2) after AP

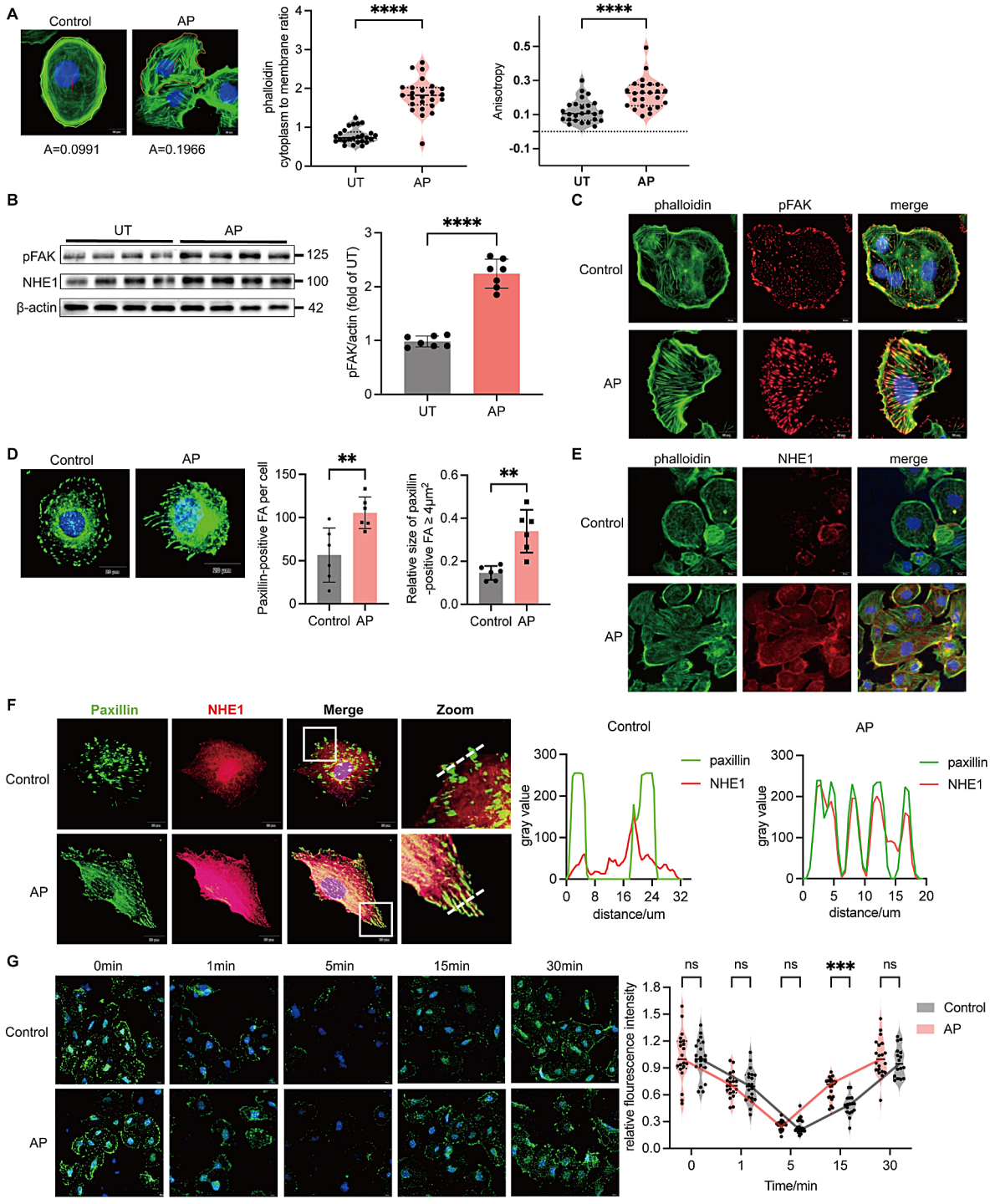

Fig. 8 The effect of AP on NHE1 aggregation at FA and activation of FA function. (**A**) F-actin (green, Phalloidin-FITC) staining of AP treated HK2 cells. Quantitative analysis was conducted to determine the ratio of F-actin in the cell membrane to the cytoplasm and the anisotropy of the cytoskeleton ($n > 24$). (**B**) Immunoblots of phosphorylation level of pFAK(Y397) and quantitative analysis after AP ($n = 8$). (**C**) Immunofluorescence revealed extensive colocalization of pFAK (red, anti-pFAK) and F-actin (green, Phalloidin-FITC) in AP treated HK2 cells. (**D**) Immunofluorescence staining of paxillin (green, anti-paxillin, FA marker) was performed in AP treated HK2 cells. Quantitative analysis was conducted to determine the number and size of focal adhesions within each cell ($n = 6$). FAs with an area exceeding 4 μm^2 were classified as mature FAs. (**E**-**F**) Immunofluorescence showed extensive colocalization of NHE1 (red, anti-NHE1) and F-actin (green, Phalloidin-FITC; E) and paxillin (green, anti-paxillin; F) in AP treated HK2 cells. (**G**) HK2 cells were treated with 10 μM Nocodazole for AP for 30 min to temporarily inhibit FA turnover. Immunofluorescence staining of pFAK (green, anti-pFAK) was performed at 0 min, 1 min, 5 min, 15 min, and 30 min after the withdraw of Nocodazole. All data are expressed as mean ± SEM. Asterisks denote statistical significance: *$p < 0.05$, **$p<0.01$, ***$p<0.001$, ****$p<0.0001$. Significance testing was performed using unpaired Student's t-test

treatment (Fig. 8D). Previous studies have shown that NHE1, localized at the leading edge of migrating cells, promotes lamellipodia extension and actin cytoskeletal polymerization by regulating local pH and volume. Consistently, our immunofluorescence analysis revealed significant colocalization of NHE1 with the cytoskeleton and with Paxillin at FAs following AP (Fig. 8E, F). This co-localization phenomenon was further validated in primary proximal tubular epithelial cells (Figure S7). The turnover rate of FAs is a key indicator of their function. To analyze FA turnover, pFAK staining was performed at multiple time points before and after the withdrawal of Nocodazole (a drug that disrupts microtubule dynamics). Notably, no significant difference was observed in the average pFAK fluorescence intensity between the two groups at 1 and 5 min after drug withdrawal. However, the AP group displayed a faster recovery of average pFAK fluorescence intensity 15 min after drug withdrawal (Fig. 8G). This finding suggests that AP promotes the accumulation of FAK and NHE1 at FAs, potentially enhancing FA function.

To investigate the functional consequences of AP, we further assessed its effects on HK2 cell migration, adhesion, and cytoskeletal structure. H/R treatment significantly impaired the migration and adhesion abilities of HK2 cells. Notably, AP treatment rescued these H/R-induced suppressions of cell mobility (Fig. 9A, B). However, the protective effects of AP were counteracted by the NHE1 inhibitor Cariporide. To verify the role of NOX4-mediated ROS production in AP's effects on cell migration and adhesion, NAC, MitoQ, and GLX351322 were employed during AP treatment. The application of both NAC and GLX351322 effectively abolished the AP-induced increase in HK2 cell motility, while MitoQ had no significant impact (Fig. 9C, D). The F/G actin ratio, an indicator of actin polymerization, was measured to assess the extent of cytoskeletal remodeling. Our findings revealed a decreased F/G ratio after H/R, suggesting actin depolymerization and cytoskeletal damage. However, AP treatment resulted in a significant upregulation of the F/G ratio, indicating reduced H/R-induced cytoskeletal damage (Fig. 9E). In *vivo* analysis of the I/R model revealed significant cytoskeletal damage and loss in renal tubular cells. Conversely, the cytoskeleton in the IPC group was relatively well-preserved (Fig. 9F).

In conclusion, our data collectively demonstrate that AP triggers actin cytoskeleton remodeling in HK2 cells. This remodeling enhances cellular functions such as migration, adhesion, and focal adhesion turnover, mediated by the FAK-NOX4-NHE1 signaling pathway.

Discussion

This study investigated the phenomenon of acidic preconditioning in renal tubular epithelial cells, demonstrating that pre-treating cells with an acidic medium followed by a return to normal medium effectively reduces damage caused by H/R. The underlying mechanism involves changes in pH_i after acid treatment. These changes trigger fluctuations in the phosphorylation level of FAK Y397, acting as a critical switch for AP. This switch leads to a cascade of events: NOX4-mediated ROS production, upregulation of NHE1 expression, and the accumulation of both proteins at focal adhesions. These events promote cytoskeletal restructuring, enhancing cellular adhesion and migration. Ultimately, AP improves cellular resilience against H/R by maintaining pH homeostasis and cytoskeletal integrity.

The renal proximal tubule epithelium plays a vital role in maintaining body acid-base homeostasis through its robust transport system. This system tightly regulates pH_i to a constant level, which is critical for cellular function and survival. However, a key vulnerability of this system is its sensitivity to changes in pH_e. Ischemia-reperfusion injury in the kidney leads to a significant decrease in pH_e. pH_i also undergoes rapid changes, exhibiting a transient drop following ischemia and early reperfusion, followed by a return and eventual elevation above control values after 45 min of reperfusion [26]. Notably, an alkaline intracellular environment promotes the proliferation and repair of proximal tubule cells [27]. Therefore, adaptation of pH_i to counteract extracellular acidification is crucial for post-injury recovery. Emerging evidence suggests that ischemic preconditioning is an effective strategy to induce pH_i adaptation and protect against myocardial, nervous system, and pulmonary injury. However, the impact of IPC on acute ischemic renal injury remains to be fully elucidated. In the present study, we demonstrate that IPC leads to renal tissue acidification and, importantly, intracellular acid adaptation in vivo. To further investigate the protective role of IPC, we tested various durations of acid treatment and recovery times. We found that acidic exposure (pH 6.6) for 12 h, followed by a 6-hour recovery period, effectively induced intracellular acid adaptation and reduced subsequent H/R injury in both HK2 cells and primary mouse renal tubular epithelial cells (Figs. 1 and 2).

NHE1 is a ubiquitously expressed protein that regulates pH_i by exchanging extracellular Na^+ for intracellular H^+ in a 1:1 ratio. In carcinoma cells, NHE1 overexpression serves as a molecular mechanism for tumor cells to counteract acidic microenvironments, promoting intracellular alkalization. This, in turn, enhances cell resistance to apoptosis and facilitates invasion and metastasis [28]. Recent studies have demonstrated the importance of NHE1 upregulation in post-acid stimulation adaptation

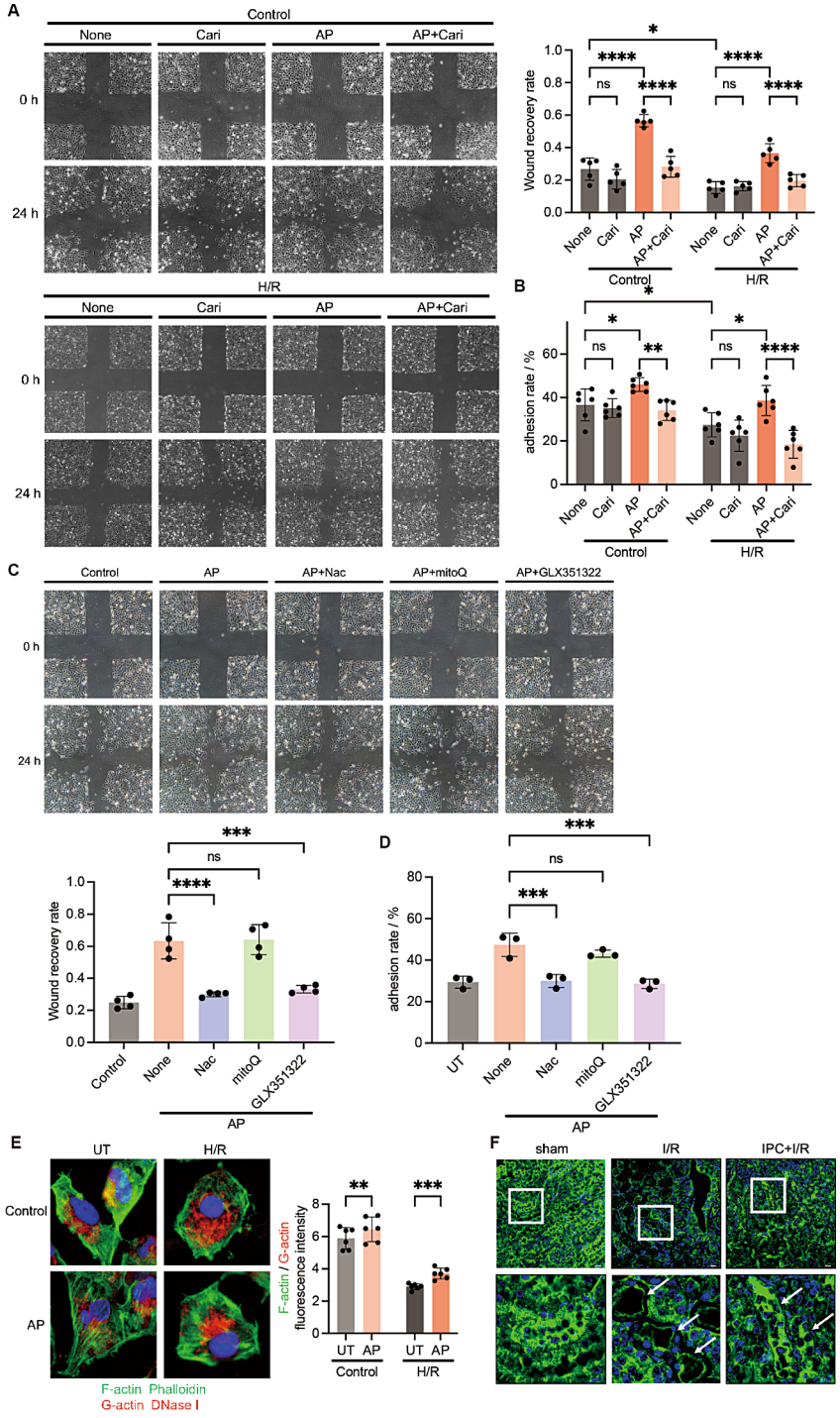

Fig. 9 AP promotes cytoskeleton remodeling and enhances cell migration and adhesion. (**A**) A wound heal test was conducted on control and AP treated HK2 cells in presence of 0.5 μM Cariporide with or without H/R treatment ($n=5$). The scratches were photographed immediately and 24 h after scratching. (**B**) Cell adhesion assay on control and AP treated HK2 cells in presence of 0.5 μM Cariporide with or without H/R treatment by celltilter Cell Viability Assay ($n=6$). (**C**) A wound heal test was conducted on HK2 cells treated with 5mM NAC, 5μM mitoQ and 10μM GLX351322 during the acidic treatment phase of AP ($n=5$). The scratches were photographed immediately and 24 h after scratching. (**D**) Cell adhesion assay on HK2 cells treated with 5mM NAC, 5μM mitoQ and 10μM GLX351322 during the acidic treatment phase of AP by celltilter Cell Viability Assay ($n=6$). (**E**) F-actin (green, Phalloidin-FITC) and G-actin (red, Alexa Fluor 594 DNase I) staining of AP treated HK2 cells with or without H/R treatment. Quantitative analysis of the fluorescence intensity ratio of F-actin and G-actin was conducted ($n=6$). (**F**) Immunofluorescence staining of β-actin (green, anti-β-actin) in paraffin sections of mouse kidneys from I/R and IPC + I/R mice. The white arrows indicate tubules with disrupted actin cytoskeleton. All data are expressed as mean ± SEM. Asterisks denote statistical significance: *$p<0.05$, **$p<0.01$, ***$p<0.001$, ****$p<0.0001$. Significance testing was performed using One-way ANOVA followed by Sidak's post test

within cardiac ventricular myocytes [5]. In healthy kidneys, NHE1 is primarily expressed in the collecting tubule intercalated cells. However, following I/R injury, NHE1 expression is upregulated in renal proximal tubular epithelial cells. Notably, ischemic preconditioning further promotes NHE1 expression in these cells, contributing to the alleviation of I/R-induced intracellular acidification (Fig. 3). In vitro experiments revealed that AP could elevate both NHE1 expression and activity in HK2 cells while enhancing the recovery rate of pH_i in response to H/R injury. Importantly, inhibition or knockout of NHE1 disrupted this intracellular acid adaptation process, abolishing the protective effect of AP (Fig. 3). These findings substantiate that increased NHE1 protein abundance and activity contribute to AP-induced acid adaptation.

Our findings suggest that NHE1 activation is triggered by the decrease in pH_i caused by AP. This is supported by the observation that acidification reversal using a low-chloride medium abolished NHE1 activation (Fig. 4). Interestingly, we observed co-localization and interaction between NHE1 and the pH_i sensor FAK at the cell cytoskeleton and focal adhesion sites (Fig. 7). NHE1, primarily located on the basolateral membrane, exhibits a longer half-life and responsiveness to diverse extracellular stimuli. This makes it well-suited to enable tubular cells to adapt to adverse conditions. Furthermore, NHE1 possesses a longer cytoplasmic carboxyl-terminal domain, anchoring it to the cytoskeleton and acting as a scaffold for various signaling molecules involved in cell survival, proliferation, migration, and adhesion. Multiple studies have revealed a complex regulatory relationship between NHE1 and the Rho family of small GTPases (RhoA, Cdc42, and Rac1), essential for actin cytoskeleton structure and function. For example, RhoA/ROCK can regulate NHE1 activity through direct or indirect phosphorylation [29]. Conversely, Cdc42 can form a positive feedback loop with NHE1 to facilitate cell migration [30]. In migrating cells, NHE1 localizes at the leading edge of lamellipodia, coordinating with various ion channels to influence cell polarity and directional migration. This is achieved by promoting sodium influx and regulating cytoskeletal dynamics. Previous research has demonstrated that AQP2-mediated Ca^{2+}-dependent NHE1 activation is associated with migration in rat renal cortical collecting duct epithelial cells [31]. Additionally, NHE1 positioned at the rear of lamellipodia accelerates cell movement, contributing to the collective driving forces for MDCK cell migration [27, 32]. Our study revealed early dynamic changes in FAK Y397 phosphorylation following acid stimulation, with prolonged exposure leading to a sustained elevation. Notably, interfering with these fluctuations using FAK Y397 phosphorylation inhibitors, integrin agonists, or FAK knockout abolished the upregulation of NHE1 expression and activity after acidosis. Importantly, it also abolished the protective effect of acidosis against H/R injury (Fig. 5). These observations suggest that alterations in FAK Y397 phosphorylation levels may serve as the initiating event for the subsequent protective effects triggered by AP.

Reactive oxygen species play a complex and multifaceted role in organisms and cells. While excessive ROS accumulation, known as oxidative stress, contributes to various diseases, moderate ROS levels function as normal metabolic byproducts. These ROS participate in diverse signaling pathways that regulate essential processes such as cell migration, proliferation, survival, and cellular adaptation to stressors [33, 34]. ROS can directly or indirectly modulate the activity of various tyrosine kinases, including FAK, by affecting their phosphorylation levels [35, 36]. Conversely, FAK activation and its downstream signaling pathways can also lead to elevated ROS levels [37]. The present study demonstrates that interrupting the dynamic Y397 phosphorylation of FAK inhibited the AP-induced elevation of ROS (Fig. 6). These findings suggest that endogenous ROS generation may be a downstream event mediated by FAK in pH_i homeostasis. Notably, precise regulation of local pH homeostasis and membrane potential via various H^+ transport mechanisms is crucial for ROS production in multiple immune cells [38]. Studies have shown that NHE1 activation and ROS elevation are the primary mechanisms for epithelial cell defense against acidic environments [39]. Furthermore, ROS can modulate NHE1 expression at the transcriptional level by directly activating the NHE1 promote [40]. Our results support this notion, as ROS inhibition counteracted the upregulation of NHE1 expression and activity, as well as the protective effects of AP. This confirms the role of ROS in AP-induced pH_i adaptation through NHE1 activation.

H_2O_2 and $O_2^{\bullet-}$ are the primary signaling molecules within the redox signaling pathway. They originate mainly from the mitochondrial electron transport chain, NADPH oxidases (NOX), xanthine oxidase, and nitric oxide synthase. NOX enzymes are considered the major source of ROS generation in various non-phagocytic cells under physiological and stress conditions. The NOX family comprises seven members (NOX1-5) and two dual oxidases (Duox1 and 2) [41, 42]. Notably, NOX4 can persistently generate H_2O_2 within diverse subcellular structures, including the nucleus, endoplasmic reticulum, mitochondria, cell membrane, and focal adhesions [43]. NOX4, also known as RENOX due to its initial discovery and high abundance in the kidney, primarily localizes within proximal tubular epithelial cells and exhibits minimal distribution among cellular components within the renal glomerulus [44]. In a physiological state, NOX4 likely plays a role in regulating renal electrolyte transport

by affecting or coordinating multiple ion channels. The involvement of NOX4 in renal diseases is multifaceted. In diabetic kidney disease, NOX4-mediated ROS generation is recognized as a significant contributor to renal damage, leading to injuries in mesangial cells, podocytes, renal tubular epithelial cells, and the development of interstitial fibrosis. NOX4 also plays a critical role in the development and progression of AKI induced by ischemia-reperfusion, cisplatin, and sepsis [45, 46]. However, in specific contexts, particularly ischemia-reperfusion-induced AKI, a moderate upregulation of NOX4 can enhance the cells' ability to cope with adverse stress, thereby exerting a protective effect on the kidney [47]. These findings suggest that the impact of NOX4 in diseases varies depending on factors such as the disease type and stage, NOX4 expression levels in different cell types, and its subcellular localization. In the present study, we observed sustained elevation of ROS levels during AP. The upregulation of NHE1 expression after AP and its protective effect against H/R injury were significantly inhibited by both the ROS scavenger N-acetyl-L-cysteine (NAC) and selective NOX4 inhibitors (Fig. 7). Conversely, drugs targeting mitochondrial ROS did not exhibit the same effects. Interestingly, FAK inhibition effectively suppressed AP-induced ROS elevation but was ineffective against exogenous H_2O_2-induced ROS elevation. Furthermore, in immune cells like macrophages and neutrophils, NOX-mediated local ROS production often coincides with the activation of multiple acid extrusion mechanisms to prevent intracellular acidification [48]. These observations suggest that NOX4-mediated ROS production outside the mitochondria may play an intermediary role in AP-induced pH_i adaptation.

Maintaining cytoskeletal integrity, cell migration, and adhesion capacities in tubular epithelial cells is directly linked to cell survival and tissue repair following AKI [16, 49]. Studies have demonstrated that acidic environments can elevate FAK Y397 phosphorylation levels in tumor cells, leading to remodeling of the cellular actin cytoskeleton, localized adhesion turnover, enhanced cell migration, and ultimately promoting tumor cell invasiveness [50]. Our results revealed that AP treatment in HK2 cells induced rearrangement of the actin cytoskeleton, with actin bundles transforming into stress fibers, increased anisotropy, and the formation of spike-like structures (Fig. 8). This actin cytoskeleton reconstruction likely coincides with the assembly and maturation of focal adhesions. Further investigations revealed that AP stimulated the formation of a complex consisting of FAK, NOX4, and NHE1 within FAs. Previous reports have shown that NOX4 localized at FAs and the cytoskeleton in monocytes and macrophages enhances cell adhesion and migration by promoting FAK and paxillin phosphorylation and actin S-glutathionylation [51]. Similarly, another study demonstrated that NOX4 in vascular smooth muscle cells directly increases local ROS levels at subcellular structures like FAs and the cytoskeleton. This promotes cell adhesion by oxidizing F-actin, recruiting vinculin, and accelerating FA formation and maturation to facilitate cell migration [52]. Notably, inhibition of either NHE1 or NOX4 prevented the enhancement of cell migration and adhesion (Fig. 9). These findings suggest that AP triggers the formation of a microdomain within FAs composed of FAK, NOX4, and NHE1. This complex likely plays a role in pHi adaptation and cytoskeletal remodeling, ultimately enhancing cell motility.

Conclusion

This study investigates the phenomenon of acidic preconditioning in HK2 human renal proximal tubule epithelial cells and explores the underlying mechanisms. Exposure to an acidic medium triggers a transient, pH_i-dependent fluctuation in FAK Y397 phosphorylation levels. These early changes likely serve as initiating events in AP, leading to NOX4-mediated ROS production and subsequent upregulation of NHE1 expression. Upregulated NHE1 then acts to restore and maintain pH_i homeostasis. Furthermore, we observed co-localization of NOX4 and NHE1 within FAs. This spatial association suggests a synergistic role for these proteins in promoting cytoskeletal remodeling and enhancing cell adhesion and migration capabilities. These combined effects ultimately improve the ability of HK2 cells to withstand subsequent H/R injury and alleviate associated cellular damage.

Supplementary Information

The online version contains supplementary material available at https://doi.org/10.1186/s12964-024-01773-w.

Supplementary Material 1

Supplementary Material 2

Author contributions

B.S., N.N.S. and X.Q.D conceived and designed the project. N.N.S, A.N.C., J.Z., Z.X.Y., J.T. and Y.F. contributed to the experimental design. A.N.C., J.Z., Z.X.Y., Y.F.L., W.Z.C., Y.X.S., Q.Y.G., S.F.Q., X.P.L., D.Z., S.Z., Z.P.Z., Y.Y. and K.L.S performed experiments. N.N.S. and A.N.C performed data analysis. J.Z. and Z.X.Y. are designated the first co-author, as they began the project and per-form all long-term in experiments. B.S., N.N.S., J.T., Y.F. and X.Q.D acquired fundings. B.S., N.N.S. and X.Q.D wrote the manuscript with input and review by all authors. All authors provided feed-back and approved the final manuscript.

Data availability

No datasets were generated or analysed during the current study.

Declarations

Competing interests

The authors declare no competing interests.

Author details

[1]Department of Nephrology, Zhongshan Hospital, Fudan University, Shanghai Medical Center of Kidney, Shanghai Institute of Kidney and

Dialysis, Shanghai Key Laboratory of Kidney and Blood Purification, Hemodialysis Quality Control Center of Shanghai, Shanghai, China
[2]Department of Nephrology, Xiamen Branch, Zhongshan Hospital, Fudan University, Xiamen, China
[3]Fudan Zhangjiang Institute, Shanghai, China
[4]Division of Nephrology, Zhongshan Hospital, Fudan University, Shanghai, PR China

Received: 30 January 2024 / Accepted: 30 July 2024
Published online: 08 August 2024

References

1. Ghosh S, Lai JY. Recent advances in the design of intracellular pH sensing nanoprobes based on organic and inorganic materials. Environ Res. 2023;237(Pt 2):117089.
2. Johmura Y, et al. Senolysis by glutaminolysis inhibition ameliorates various age-associated disorders. Science. 2021;371(6526):265–70.
3. Michl J, et al. Acid-adapted cancer cells alkalinize their cytoplasm by degrading the acid-loading membrane transporter anion exchanger 2, SLC4A2. Cell Rep. 2023;42(6):112601.
4. Simkhovich BZ, et al. Transient pre-ischemic acidosis protects the isolated rabbit heart subjected to 30 minutes, but not 60 minutes, of global ischemia. Basic Res Cardiol. 1995;90(5):397–403.
5. Wilson AD et al. Acidic environments trigger intracellular H+-sensing FAK proteins to re-balance sarcolemmal acid-base transporters and auto-regulate cardiomyocyte pH. Cardiovascular Res, 2022.
6. Wilson AD, et al. Acidic environments trigger intracellular H+-sensing FAK proteins to re-balance sarcolemmal acid-base transporters and auto-regulate cardiomyocyte pH. Cardiovasc Res. 2022;118(14):2946–59.
7. Bocanegra V, et al. RhoA and MAPK signal transduction pathways regulate NHE1-dependent proximal tubule cell apoptosis after mechanical stretch. Am J Physiol Ren Physiol. 2014;307(7):F881–9.
8. Pedersen SF, Counillon L. The SLC9A-C mammalian na(+)/H(+) Exchanger Family: molecules, mechanisms, and physiology. Physiol Rev. 2019;99(4):2015–113.
9. Parker MD, Myers EJ, Schelling JR. Na+-H + exchanger-1 (NHE1) regulation in kidney proximal tubule. Cell Mol Life Sci. 2015;72(11):2061–74.
10. Cardoso VG, et al. Angiotensin II-induced podocyte apoptosis is mediated by endoplasmic reticulum stress/PKC-δ/p38 MAPK pathway activation and trough increased na(+)/H(+) exchanger isoform 1 activity. BMC Nephrol. 2018;19(1):179.
11. Ganz MB, Hawkins K, Reilly RF. High glucose induces the activity and expression of na(+)/H(+) exchange in glomerular mesangial cells. Am J Physiol Ren Physiol. 2000;278(1):F91–6.
12. Li P, et al. Inhibition of NA(+)/H(+) exchanger 1 attenuates renal Dysfunction Induced by Advanced Glycation End products in rats. J Diabetes Res. 2016;2016:p1802036.
13. Wang Z, et al. Ischemic-reperfusion injury in the kidney: overexpression of colonic H+-K+-ATPase and suppression of NHE-3. Kidney Int. 1997;51(4):1106–15.
14. Yamashita J, et al. Role of Na+/H + exchanger in the pathogenesis of ischemic acute renal failure in mice. J Cardiovasc Pharmacol. 2007;49(3):154–60.
15. Parsons JT. Focal adhesion kinase: the first ten years. J Cell Sci. 2003;116(Pt 8):1409–16.
16. Humphreys BD, et al. Intrinsic epithelial cells repair the kidney after injury. Cell Stem Cell. 2008;2(3):284–91.
17. Alderliesten M, et al. Extracellular signal-regulated kinase activation during renal ischemia/reperfusion mediates focal adhesion dissolution and renal injury. Am J Pathol. 2007;171(2):452–62.
18. Qin Y, et al. Focal adhesion kinase signaling mediates acute renal injury induced by ischemia/reperfusion. Am J Pathol. 2011;179(6):2766–78.
19. Yamashita N, et al. Intratubular epithelial-mesenchymal transition and tubular atrophy after kidney injury in mice. Am J Physiol Ren Physiol. 2020;319(4):F579–91.
20. Choi CH, et al. pH sensing by FAK-His58 regulates focal adhesion remodeling. J Cell Biol. 2013;202(6):849–59.
21. Xu X, et al. Delayed ischemic preconditioning contributes to renal protection by upregulation of miR-21. Kidney Int. 2012;82(11):1167–75.
22. Xu S, et al. Nuclear farnesoid X receptor attenuates acute kidney injury through fatty acid oxidation. Kidney Int. 2022;101(5):987–1002.
23. Mena HA, et al. Acidic preconditioning improves the proangiogenic responses of endothelial colony forming cells. Angiogenesis. 2014;17(4):867–79.
24. Cencioni C, et al. Ex vivo acidic preconditioning enhances bone marrow ckit cell therapeutic potential via increased CXCR4 expression. Eur Heart J. 2013;34(26):2007–16.
25. Boudaoud A, et al. FibrilTool, an ImageJ plug-in to quantify fibrillar structures in raw microscopy images. Nat Protoc. 2014;9(2):457–63.
26. Holloway JC, et al. Renal acid-base metabolism after ischemia. Kidney Int. 1986;29(5):989–94.
27. Cornejo M, et al. Arsenic trioxide-increased MDCK cells proliferation requires activator protein 1-mediated increase of the sodium/proton exchanger 1 activity. Biochim Biophys Acta Mol Basis Dis. 2021;1867(1):165977.
28. Wang B, et al. IDH1 K224 acetylation promotes colorectal cancer via miR-9-5p/NHE1 axis-mediated regulation of acidic microenvironment. iScience. 2023;26(7):107206.
29. Denker SP, Barber DL. Cell migration requires both ion translocation and cytoskeletal anchoring by the Na-H exchanger NHE1. J Cell Biol. 2002;159(6):1087–96.
30. Frantz C, et al. Positive feedback between Cdc42 activity and H + efflux by the Na-H exchanger NHE1 for polarity of migrating cells. J Cell Biol. 2007;179(3):403–10.
31. Di Giusto G, et al. Aquaporin-2 and na(+) /H(+) exchanger isoform 1 modulate the efficiency of renal cell migration. J Cell Physiol. 2020;235(5):4443–54.
32. Jensen HH, et al. The na(+) /H(+) exchanger NHE1 localizes as clusters to cryptic lamellipodia and accelerates collective epithelial cell migration. J Physiol. 2019;597(3):849–67.
33. Sies H, Jones DP. Reactive oxygen species (ROS) as pleiotropic physiological signalling agents. Nat Rev Mol Cell Biol. 2020;21(7):363–83.
34. Sies H. Oxidative eustress: on constant alert for redox homeostasis. Redox Biol. 2021;41:101867.
35. Fernandes GV, et al. Osteoblast adhesion dynamics: a possible role for ROS and LMW-PTP. J Cell Biochem. 2014;115(6):1063–9.
36. Kim YM, Muthuramalingam K, Cho M. Redox Regulation of NOX isoforms on FAK((Y397))/SRC((Y416)) phosphorylation driven epithelial-to-mesenchymal transition in malignant cervical epithelial cells. Cells, 2020. 9(6).
37. Wang Y, et al. Focal adhesion kinase inhibitor inhibits the oxidative damage Induced by Central venous catheter via abolishing focal adhesion kinase-protein kinase B pathway activation. Biomed Res Int. 2021;2021:p6685493.
38. Capasso M, DeCoursey TE, Dyer MJ. pH regulation and beyond: unanticipated functions for the voltage-gated proton channel, HVCN1. Trends Cell Biol. 2011;21(1):20–8.
39. Park SY, et al. Intrinsic resistance triggered under acid loading within normal esophageal epithelial cells: NHE1- and ROS-mediated survival. J Cell Physiol. 2015;230(7):1503–14.
40. Akram S, et al. Reactive oxygen species-mediated regulation of the Na+-H + exchanger 1 gene expression connects intracellular redox status with cells' sensitivity to death triggers. Cell Death Differ. 2006;13(4):628–41.
41. Cheng G, et al. Homologs of gp91phox: cloning and tissue expression of Nox3, Nox4, and Nox5. Gene. 2001;269(1–2):131–40.
42. Kawahara T, Quinn MT, Lambeth JD. Molecular evolution of the reactive oxygen-generating NADPH oxidase (Nox/Duox) family of enzymes. BMC Evol Biol. 2007;7:109.
43. Martyn KD, et al. Functional analysis of Nox4 reveals unique characteristics compared to other NADPH oxidases. Cell Signal. 2006;18(1):69–82.
44. Geiszt M, et al. Identification of renox, an NAD(P)H oxidase in kidney. Proc Natl Acad Sci U S A. 2000;97(14):8010–4.
45. Yang Q, et al. Nox4 in renal diseases: an update. Free Radic Biol Med. 2018;124:466–72.
46. Gorin Y, Wauquier F. Upstream regulators and downstream effectors of NADPH oxidases as novel therapeutic targets for diabetic kidney disease. Mol Cells. 2015;38(4):285–96.
47. Nlandu-Khodo S, et al. NADPH oxidase 4 deficiency increases tubular cell death during acute ischemic reperfusion injury. Sci Rep. 2016;6:38598.
48. DeCoursey TE. The intimate and controversial relationship between voltage-gated proton channels and the phagocyte NADPH oxidase. Immunol Rev. 2016;273(1):194–218.
49. Kusaba T, et al. Differentiated kidney epithelial cells repair injured proximal tubule. Proc Natl Acad Sci U S A. 2014;111(4):1527–32.
50. Li S, et al. Acidic pHe regulates cytoskeletal dynamics through conformational integrin β1 activation and promotes membrane protrusion. Biochim Biophys Acta Mol Basis Dis. 2018;1864(7):2395–408.

51. Lee CF, et al. Regulation of Monocyte Adhesion and Migration by Nox4. PLoS ONE. 2013;8(6):e66964.
52. Vukelic S, et al. NOX4 (NADPH oxidase 4) and Poldip2 (polymerase δ-Interacting protein 2) induce filamentous actin oxidation and promote its Interaction with Vinculin during integrin-mediated cell adhesion. Arterioscler Thromb Vasc Biol. 2018;38(10):2423–34.

Publisher's Note